

Searching for Extra Z' from Strings and Other Models at the LHC with Leptoproduction

Claudio Corianò ^{a,b}, Alon E. Faraggi ^c and Marco Guzzi^a

^a*Dipartimento di Fisica, Università del Salento, and
INFN Sezione di Lecce, Via Arnesano 73100 Lecce, Italy*

^b*Department of Physics and Institute of Plasma Physics
University of Crete, 71003 Heraklion, Greece*

^c*Department of Mathematical Sciences,
University of Liverpool, Liverpool L69 7ZL, United Kingdom*

Abstract

Discovery potentials for extra neutral interactions at the Large Hadron Collider in forthcoming experiments are analyzed using resonant leptoproduction. For this purpose we use high precision next-to-next-to-leading order (NNLO) determinations of the QCD background in this channel, at the tail of the Drell-Yan distributions, in the invariant mass region around $0.8 < Q < 2.5$ TeV. We focus our analysis primarily on a novel string-inspired Z' , obtained in left-right symmetric free fermionic heterotic string models and whose existence at low energies is motivated by its role in suppressing proton decay mediation. We analyze the parametric dependence of the predictions and perform comparison with other models based on bottom up approaches, that are constructed by requiring anomaly cancellation and enlarged Higgs structure. We show that the results are not particularly sensitive to the specific charge assignments. This may render quite difficult the extraction of significant information from the forward-backward asymmetries on the resonance, assuming that these are possible due to a sizeable width. The challenge to discover extra (non anomalous) Z' in this kinematic region remains strongly dependent on the size of the new gauge coupling. Weakly coupled extra Z' will not be easy to identify even with a very good theoretical determination of the QCD background through NNLO.

1 Introduction

The search for neutral currents mediated by extra gauge bosons (Z') at the Large Hadron Collider will gather considerable attention in the next few years [1]. Additional Abelian gauge interactions arise frequently in many extensions of the Standard Model, like in left–right symmetric models, in Grand Unified Theories (GUTs) and in string inspired constructions [1]. It has also been suggested that the existence of a low scale Z' may account for the suppression of proton decay mediating operators in supersymmetric theories and otherwise [2, 3, 4]. Abelian gauge structures may also play a considerable role in fixing the structure of the flavor sector, for instance in pinning down the neutrinos mass matrix. Anomaly cancellation conditions, when supported also by an extended Higgs and fermion family structure - for instance by the inclusion of right-handed neutrinos - may allow non-sequential solutions (i.e. charge assignments which are not proportional to the hypercharge) that are phenomenologically interesting and could be studied by ATLAS and CMS. Furthermore, within left–right symmetric models, and their underlying $SO(10)$ embedding, the global baryon minus lepton number ($B - L$) of the Standard Model is promoted to a local symmetry. Abelian gauge extensions are therefore among the most well motivated extensions of the Standard Model. For these reasons, the identification of the origin of the extra neutral interaction in future collider experiments will be an important and challenging task. In particular, measurements of the charge asymmetries - both for the rapidity distributions and for the related total cross section - and of the forward-backward asymmetries, may be a way to gather information about the structure of these new neutral currents interactions, although in the models that we have studied this looks pretty difficult, given the low statistics.

As an extra Z' is common in model building, the differences among the various constructions may remain unresolved, unless additional physical requirements are imposed on these models in order to strengthen the possibility for their unique identification. In this work we analyze the potential for the discovery of an extra Z' arising in a specific string construction, which is motivated not only by an anomaly-free structure, as in most of the bottom–up models considered in the previous literature, but with some additional requirements coming from an adequate suppression of proton decay mediation. Bottom up approaches based only on anomaly cancellation are, in this respect, less constraining compared to models derived either from a string construction or from theories of grand unification (GUTs) and can only provide a basic framework within which to direct the experimental searches. At the same time the search for extra neutral interactions has to proceed in some generality and be unbiased, looking for resonances in several complementary channels. In this work we will investigate the relation between more constrained and

less constrained searches of extra neutral gauge bosons by choosing as a channel leptoproduction and proceed with a comparison of some proposals that have been presented in the recent literature. Our main interest is focused around an extra Z' which has been derived using the free fermionic formulation of string theory in a specific class of left–right symmetric string models. The new abelian structure is determined not just as an attempt to satisfy some additional physical requirements, on which we elaborate below, but is naturally derived from a class of string models which have been extensively studied in detail in the past two decades [6, 7, 8, 9].

Our paper is organized as follows: in section 2 we discuss the origin of Z' in heterotic–string models. We discuss in some details the origin of the charge assignment under the Z' , which is motivated from proton decay considerations and differs from those that have traditionally been discussed in the literature. Then we move to define the conventions in regard to the charge assignments and the Higgs structure of the models that we consider, which are characterized by a gauge structure which enlarges the gauge group of the Standard Model by one extra $U(1)$. Our numerical analysis of the invariant mass distributions for leptoproduction is performed by varying both the coupling of the extra $U(1)$ and the mass of the new gauge boson. The dependence on these parameters of the models that we discuss are studied rather carefully in a kinematic region which can be accessed at the LHC. We compare these results with those obtained for a group of 4 different models, introduced in [10], for which we perform a similar analysis using leptoproduction. From this analysis it is quite evident that the search for extra neutral currents at the LHC is a rather difficult enterprise in leptoproduction, unless the coupling of the new gauge interaction is quite sizeable.

2 Heterotic–string inspired Z'

Phenomenological string models can be built in the heterotic–string or, using brane constructions, in the type I string. The advantage of the former is that it produces states in spinorial representations of the gauge group, and hence allows for the $SO(10)$ embedding of the matter spectrum. The ten dimensional supersymmetric heterotic–string vacua give rise to effective field theories that descend from the $E_8 \times E_8$ or $SO(32)$ gauge groups. The first case gives rise to additional Z' s that arise in the $SO(10)$ and E_6 extensions of the Standard Model, and are the cases mostly studied in the literature [1]. A basis for the extra Z' arising in these models is formed by the two groups $U(1)_\chi$ and $U(1)_\psi$ via the decomposition $E_6 \rightarrow SO(10) \times U(1)_\psi$ and $SO(10) \rightarrow SU(5) \times U(1)_\chi$ [1]. Additional, flavor non–universal $U(1)$'s, may arise in heterotic $E_8 \times E_8$ string models from the $U(1)$ currents in the Cartan subalgebra of the four dimensional gauge group, that are external to E_6 . Non–universal

Z 's typically must be beyond the LHC reach, to avoid conflict with Flavor Changing Neutral Currents (FCNC) constraints. Recently [4] a novel Z' in quasi-realistic string models that do not descend from the heterotic $E_8 \times E_8$ string has been identified. Under the new $U(1)$ symmetry left-handed components and right-handed components in the 16 spinorial $SO(10)$ representation, of each Standard Model generation, have charge $-1/2$ and $+1/2$, respectively. As a result, the extra $U(1)$ is family universal and anomaly free. It arises in left-right symmetric string models [9], in which the $SO(10)$ symmetry is broken directly at the string level to $SU(3) \times U(1)_{B-L} \times SU(2)_L \times SU(2)_R \times U(1)_{Z'} \times U(1)^n \times \text{hidden}$ [9]. The $U(1)^n$ are flavor dependent $U(1)$ s that are broken near the string scale. The Standard Model matter states are neutral under the hidden sector gauge group, which in these string models is typically a rank eight group. It is important to note that the fact that the spectrum is derived from a string vacuum that satisfies the modular invariance constraints, establishes that the model is free from gauge and gravitational anomalies. The pattern of $U(1)_{Z'}$ charges in the quasi-realistic string models of ref. [9] does not arise in related string models in which the $SO(10)$ symmetry is broken to the $SU(5) \times U(1)$ [6], the $SO(6) \times SO(4)$ [7], or $SU(3) \times SU(2) \times U(1)^2$ [8], subgroups. The reason for the distinction of the left-right symmetric string models is the boundary condition assignment to the world-sheet free fermions that generate the $SO(10)$ symmetry in the basis vectors that break the $SO(10)$ symmetry to one of its subgroups. The world-sheet fermions that generate the rank eight observable gauge group in the free fermionic models are denoted by $\{\bar{\psi}^{1,\dots,5}, \bar{\eta}^{1,2,3}\}$, where $\bar{\psi}^{1,\dots,5}$ generate an $SO(10)$ symmetry, and $\bar{\eta}^{1,2,3}$ produce three $U(1)$ currents¹. Additional observable gauged $U(1)$ currents may arise at enhanced symmetry points of the compactified six dimensional lattice. The $SO(10)$ gauge group is broken to one of its subgroups $SU(5) \times U(1)$, $SO(6) \times SO(4)$ or $SU(3) \times SU(2) \times U(1)^2$ by the assignment of boundary conditions to the set $\bar{\psi}_{\frac{1}{2}}^{1,\dots,5}$:

$$\begin{aligned}
1. \quad b\{\bar{\psi}^{1,\dots,5}\bar{\eta}^{1,2,3}\} &= \left\{ \frac{1}{2} \frac{1}{2} \frac{1}{2} \frac{1}{2} \frac{1}{2} \frac{1}{2} \frac{1}{2} \frac{1}{2} \right\} \Rightarrow SU(5) \times U(1) \times U(1)^3, & (1) \\
2. \quad b\{\bar{\psi}^{1,\dots,5}\bar{\eta}^{1,2,3}\} &= \{11100000\} \Rightarrow SO(6) \times SO(4) \times U(1)^3.
\end{aligned}$$

To break the $SO(10)$ symmetry to² $SU(3)_C \times SU(2)_L \times U(1)_C \times U(1)_L$ both steps, 1 and 2, are used, in two separate basis vectors. The breaking pattern $SO(10) \rightarrow SU(3)_C \times SU(2)_L \times SU(2)_R \times U(1)_{B-L}$ is achieved by the following assignment in two separate basis vectors

$$\begin{aligned}
1. \quad b\{\bar{\psi}^{1,\dots,5}\bar{\eta}^{1,2,3}\} &= \{11100000\} \Rightarrow SO(6) \times SO(4) \times U(1)^3, & (2) \\
2. \quad b\{\bar{\psi}^{1,\dots,5}\bar{\eta}^{1,2,3}\} &= \left\{ \frac{1}{2} \frac{1}{2} \frac{1}{2} 00 \frac{1}{2} \frac{1}{2} \frac{1}{2} \right\} \Rightarrow SU(3)_C \times U(1)_C \times SU(2)_L \times SU(2)_R \times U(1)^3
\end{aligned}$$

¹for reviews and the notation used in free fermionic string models see *e.g.* [5] and references therein.

² $U(1)_C = \frac{3}{2}U(1)_{B-L}; U(1)_L = 2U(1)_{T_{3R}}$.

The distinction between the symmetry breaking patterns in eq. (1) and eq. (2) is with respect to the charges of the Standard Model states under the three flavor dependent $U(1)$ symmetries $U(1)_{1,2,3}$ that arise from the three world-sheet fermions $\bar{\eta}^{1,2,3}$. In the free fermionic models, the states of each Standard Model generation fit into the 16 representation of $SO(10)$, and are charged with respect to one of the three flavor $U(1)$ symmetries. For the symmetry breaking pattern given in eq. (1) the charge is always $+1/2$, *i.e.*

$$Q_j(16 = \{Q, L, U, D, E, N\}) = +\frac{1}{2} \quad (3)$$

whereas for the symmetry breaking pattern in eq. (2) the charges are

$$\begin{aligned} Q_j(Q_L, L_L) &= -\frac{1}{2} \\ Q_j(Q_R = \{U, D\}, L_R = \{E, N\}) &= +\frac{1}{2} \end{aligned} \quad (4)$$

As a result in the models admitting the symmetry breaking pattern eq. (1) the combination

$$U(1)_\zeta = U(1)_1 + U(1)_2 + U(1)_3. \quad (5)$$

is anomalous, whereas in the models admitting the symmetry breaking pattern (2) it is anomaly free. The distinction between the two boundary condition assignments given in eqs. (1) and (2), and the consequent symmetry breaking patterns, is important for the following reason. Whereas the first is obtained from an $N = 4$ vacuum with $E_8 \times E_8$ or $SO(16) \times SO(16)$ gauge symmetry, arising from the $\{\bar{\psi}^{1,\dots,5}, \bar{\eta}^{1,2,3}, \bar{\phi}^{1,\dots,8}\}$ world-sheet fermions, which generate the observable and hidden sectors gauge symmetries, the second cannot be obtained from these $N = 4$ vacua, but rather from an $N = 4$ vacuum with $SO(16) \times E_7 \times E_7$ gauge symmetry, where we have included here also the symmetry arising from the compactified lattice at the enhanced symmetry point. The important fact from the point of view of the Z' phenomenology in which we are interested is that the first case gives rise to the type of string inspired Z' that arises in models with an underlying E_6 symmetry. Whereas the E_6 may be broken at the string level, rather than in the effective low energy field theory, the crucial point is that the charge assignment of the Standard Model states is fixed by the underlying E_6 symmetry. The entire literature on string inspired Z' studies this type of E_6 inspired Z' . The second class, however, is novel and has not been studied in the literature. In this respect it would be interesting to examine how the symmetry breaking pattern (2) and the corresponding charge assignments (4) can be obtained in heterotic orbifold models in which one starts from a ten dimensional theory and compactifies to four dimensions, rather than starting directly with a theory in four dimensions, as is done in the free fermionic models. This understanding may

highlight the relevance of ten dimensional backgrounds that have thus far been ignored in the literature. From the point of view of the Z' phenomenology, which is our interest here, the crucial point will be to resolve between the different Z' models and the fermion charges, which will reveal the relevance of a particular symmetry breaking pattern.

The existence of the extra Z' at low energies, within reach of the LHC, is motivated by proton longevity, and the suppression of the proton decay mediating operators [2, 3, 4]. The important property of this Z' is that it forbids dimension four, five and six proton decay mediating operators. The extra $U(1)$ is anomaly free and family universal. It allows the fermions Yukawa couplings to the Higgs field and the generation of small neutrino masses via a seesaw mechanism. String models contain several $U(1)$ symmetries that suppress the proton decay mediating operators [3]. However, these are typically non-family universal. They constrain the fermion mass terms and hence must be broken at a high scale. Thus, the existence of a $U(1)$ symmetry that can remain unbroken down to low energies is highly nontrivial. The $U(1)$ symmetry in ref. [9, 4] satisfies all of these requirements. Furthermore, as the generation of small neutrino masses in the string models arises from the breaking of the $B-L$ current, the extra $U(1)$ allows lepton number violating terms, but forbids the baryon number violating terms. Hence, it predicts that R -parity is violated and its phenomenological implications for SUSY collider searches differ substantially from models in which R -parity is preserved. The charges of the Standard Model states under the Z' are displayed in table 9. Also displayed in the table are the charges under $U(1)_{\zeta'} = U_C - U_L$, which is the Abelian combination of the Cartan generators of the underlying $SO(10)$ symmetry that is orthogonal to the weak hypercharge $U(1)_Y$. The charges under the $U(1)$ combination given in eq. (5) are displayed in table 9 as well. These two $U(1)$'s are broken by the VEV that induces the seesaw mechanism, and the combination

$$U(1)_{Z'} = \frac{1}{5}U(1)_{\zeta'} - U(1)_{\zeta} \quad (6)$$

is left unbroken down to low energies in order to suppress the proton decay mediating operators. The charges of the Standard Model states under this $U(1)_{Z'}$ are displayed in table 9.

3 The interactions for $U(1)_{Z'}$

In this section we fix our conventions and describe the structure of the new neutral sector that we are going to analyze numerically in leptoproduction afterwards. The notations are the same both in the case of the string model and for the other models that we will investigate. We show in (9) the field content of the string model obtained within the free

fermionic construction discussed above. Of the 3 extra $U(1)$, we will decouple the two gauge bosons denoted by ζ, ζ' and keep only the Z' . The assumption of decoupling of these extra components are realistic if they are massive enough (> 5 TeV) so to neglect their influence on the lowest new resonance. We have chosen a mass $M_{Z'}$ around 0.8 TeV. We recall that a reasonable region where the new extra gauge boson have a chance of being detected is below the 5 TeV range.

The fermion-fermion- Z' interaction is given by

$$\sum_f z_f g_z \bar{f} \gamma^\mu f Z'_\mu, \quad (7)$$

where $f = e_R^j, l_L^j, u_R^j, d_R^j, q_L^j$ and $q_L^j = (u_L^j, d_L^j), l_L^j = (\nu_L^j, e_L^j)$. The coefficients z_u, z_d are the charges of the right-handed up and down quarks, respectively, while the z_q coefficients are the charges of the left-handed quarks. g_z is the Z' coupling constant. We can write the Lagrangean for the Z' -lepton-quark interactions as follows

$$\mathcal{L}_{Z'} = \sum_j g_z Z'_\mu \left[z_{e_R^j} \bar{e}_R^j \gamma^\mu e_R^j + z_{l_L^j} \bar{l}_L^j \gamma^\mu l_L^j + z_{u_R^j} \bar{u}_R^j \gamma^\mu u_R^j + z_{d_R^j} \bar{d}_R^j \gamma^\mu d_R^j + z_{q_L^j} \bar{Q}_L^j \gamma^\mu Q_L^j \right], \quad (8)$$

with j being the generation index. The low energy spectrum of the model, as discussed above, is assumed to be the same for the other models that we analyze in parallel. As shown in (9) the field content of the model is effectively that of the Standard Model plus 1 additional Higgs doublet. The extra scalars ϕ , and $\zeta_H, \bar{\zeta}_H$ and the right handed components N_H and \bar{N}_H are assumed to decouple. In this simplified framework, the structure of the vertex

Field	$U(1)_Y$	$U(1)_{\zeta'}$	$U(1)_\zeta$	$U(1)_{Z'}$
Q^i	$\frac{1}{6}$	$\frac{1}{2}$	$-\frac{1}{2}$	$\frac{3}{5}$
L^i	$-\frac{1}{2}$	$-\frac{3}{2}$	$-\frac{1}{2}$	$\frac{1}{5}$
U^i	$-\frac{2}{3}$	$\frac{1}{2}$	$\frac{1}{2}$	$-\frac{2}{5}$
D^i	$\frac{1}{3}$	$-\frac{3}{2}$	$\frac{1}{2}$	$-\frac{4}{5}$
E^i	1	$\frac{1}{2}$	$\frac{1}{2}$	$-\frac{2}{5}$
N^i	0	$\frac{5}{2}$	$\frac{1}{2}$	0
ϕ^i	0	0	0	0
ϕ^0	0	0	0	0
H^U	$\frac{1}{2}$	-1	0	$-\frac{1}{5}$
H^D	$-\frac{1}{2}$	1	0	$\frac{1}{5}$
N_H	0	$\frac{5}{2}$	$\frac{1}{2}$	0
\bar{N}_H	0	$-\frac{5}{2}$	$-\frac{1}{2}$	0
ζ_H	0	0	1	1
$\bar{\zeta}_H$	0	0	-1	-1

is the following

$$-\frac{ig}{4\cos\theta_W}\bar{\psi}_i\gamma^\mu(g_V^{Z,Z'}+g_A^{Z,Z'}\gamma^5)\psi V_\mu, \quad (10)$$

where V_μ denotes generically the vector boson. In the Standard Model (SM)

$$\begin{aligned} v_u^\gamma &= \frac{2}{3} & a_u^\gamma &= 0 \\ v_d^\gamma &= -\frac{1}{3} & a_d^\gamma &= 0 \\ v_u^Z &= 1 - \frac{8}{3}\sin^2\theta_W & a_u^Z &= -1 \\ v_d^Z &= -1 + \frac{4}{3}\sin^2\theta_W & a_d^Z &= 1. \end{aligned} \quad (11)$$

We need to generalize this formalism to the case of the Z' .

Our starting point is the covariant derivative in a basis where the three electrically-neutral gauge bosons $W_\mu^3, B_Y^\mu, B_z^\mu$ are

$$\hat{D}_\mu = \left[\partial_\mu - ig(W_\mu^1 T^1 + W_\mu^2 T^2 + W_\mu^3 T^3) - i\frac{g_Y}{2}\hat{Y}B_Y^\mu - i\frac{g_z}{2}\hat{z}B_z^\mu \right] \quad (12)$$

and we denote with g, g_Y, g_z the couplings of $SU(2), U(1)_Y$ and $U(1)_z$, with $\tan\theta_W = g_Y/g$. After the diagonalization of the mass matrix we have

$$\begin{pmatrix} A_\mu \\ Z_\mu \\ Z'_\mu \end{pmatrix} = \begin{pmatrix} \sin\theta_W & \cos\theta_W & 0 \\ \cos\theta_W & -\sin\theta_W & \varepsilon \\ -\varepsilon\sin\theta_W & \varepsilon\sin\theta_W & 1 \end{pmatrix} \begin{pmatrix} W_\mu^3 \\ B_\mu^Y \\ B_\mu^z \end{pmatrix} \quad (13)$$

where ε is defined as a perturbative parameter

$$\begin{aligned}
\varepsilon &= \frac{\delta M_{ZZ'}^2}{M_{Z'}^2 - M_Z^2} \\
M_Z^2 &= \frac{g^2}{4 \cos^2 \theta_W} (v_{H_1}^2 + v_{H_2}^2) [1 + O(\varepsilon^2)] \\
M_{Z'}^2 &= \frac{g_z^2}{4} (z_{H_1}^2 v_{H_1}^2 + z_{H_2}^2 v_{H_2}^2 + z_\phi^2 v_\phi^2) [1 + O(\varepsilon^2)] \\
\delta M_{ZZ'}^2 &= -\frac{gg_z}{4 \cos \theta_W} (z_{H_1}^2 v_{H_1}^2 + z_{H_2}^2 v_{H_2}^2). \tag{14}
\end{aligned}$$

Then we define

$$g = \frac{e}{\sin \theta_W} \quad g_Y = \frac{e}{\cos \theta_W}, \tag{15}$$

and we construct the W^\pm charge eigenstates and the corresponding generators T^\pm as usual

$$\begin{aligned}
W^\pm &= \frac{W_1 \mp iW_2}{\sqrt{2}} \\
T^\pm &= \frac{T_1 \pm iT_2}{\sqrt{2}}, \tag{16}
\end{aligned}$$

with the rotation matrix

$$\begin{pmatrix} W_\mu^3 \\ B_\mu^Y \\ B_\mu^z \end{pmatrix} = \begin{pmatrix} \frac{\sin \theta_W (1+\varepsilon^2)}{1+\varepsilon^2} & \frac{\cos \theta_W}{1+\varepsilon^2} & \varepsilon \frac{\cos \theta_W}{1+\varepsilon^2} \\ \frac{\cos \theta_W (1+\varepsilon^2)}{1+\varepsilon^2} & -\frac{\sin \theta_W}{1+\varepsilon^2} & \varepsilon \frac{\sin \theta_W}{1+\varepsilon^2} \\ 0 & \frac{\varepsilon}{1+\varepsilon^2} & \frac{1}{1+\varepsilon^2} \end{pmatrix} \begin{pmatrix} A_\mu \\ Z_\mu \\ Z'_\mu \end{pmatrix} \tag{17}$$

from the interaction to the mass eigenstates. Substituting these expression in the covariant derivative we obtain

$$\begin{aligned}
\hat{D}_\mu &= \left[\partial_\mu - iA_\mu \left(gT_3 \sin \theta_W + g_Y \cos \theta_W \frac{\hat{Y}}{2} \right) - ig (W_\mu^- T^- + W_\mu^+ T^+) \right. \\
&\quad \left. - iZ_\mu \left(g \cos \theta_W T_3 - g_Y \sin \theta_W \frac{\hat{Y}}{2} + g_z \varepsilon \frac{\hat{z}}{2} \right) \right. \\
&\quad \left. - iZ'_\mu \left(-g \cos \theta_W T_3 \varepsilon + g_Y \sin \theta_W \frac{\hat{Y}}{2} \varepsilon + g_z \frac{\hat{z}}{2} \right) \right] \tag{18}
\end{aligned}$$

where we have neglected all the $O(\varepsilon^2)$ terms. Sending $g_z \rightarrow 0$ and $\varepsilon \rightarrow 0$ we obtain the SM expression for the covariant derivative. The next step is to separate left and right contributions in the interactions between the fermions and the Z' boson. Hence for the quarks and the leptons we can write an interaction Lagrangean of the type

$$\mathcal{L}_{int} = \bar{Q}_L^j N_L^Z \gamma^\mu Q_L^j Z_\mu + \bar{Q}_L^j N_L^{Z'} \gamma^\mu Q_L^j Z'_\mu + \bar{u}_R^j N_{u,R}^Z \gamma^\mu u_R^j Z_\mu$$

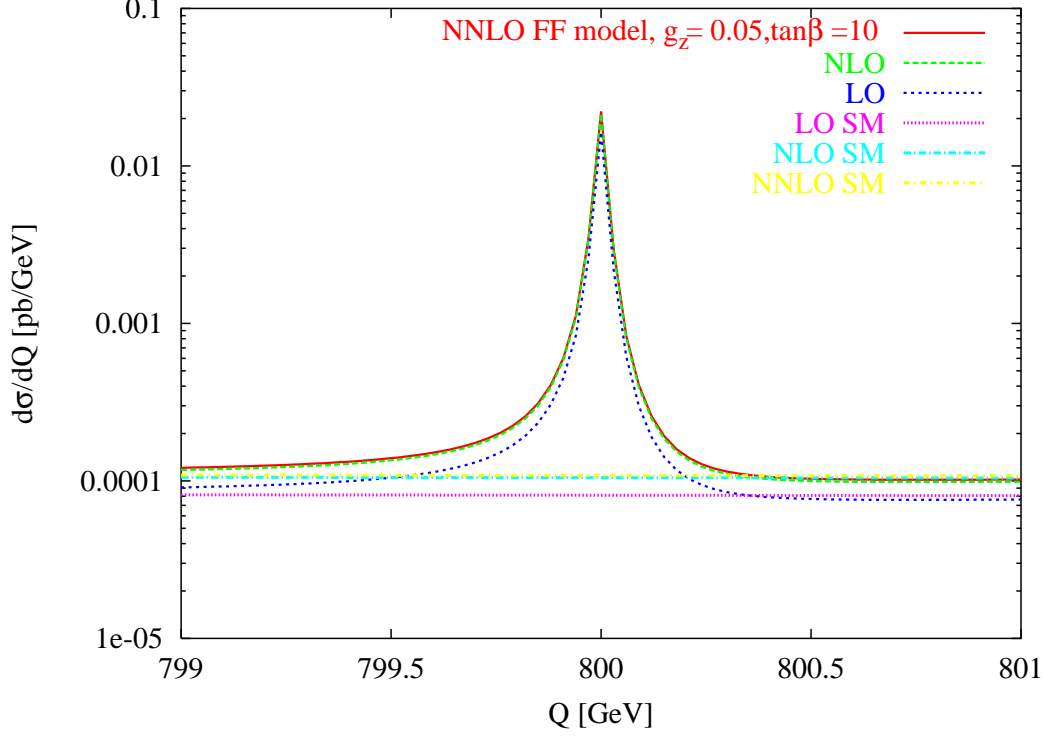


Figure 1: Plot of the LO, NLO and NNLO cross section for the free fermionic model with $M_{Z'} = 800$ GeV.

$$\begin{aligned}
& + \bar{d}_R^j N_{d,R}^Z \gamma^\mu d_R^j Z_\mu + \bar{u}_R^j N_{u,R}^{Z'} \gamma^\mu u_R^j Z'_\mu + \bar{d}_R^j N_{d,R}^{Z'} \gamma^\mu d_R^j Z'_\mu \\
& + \bar{Q}_L^j N_L^\gamma \gamma^\mu Q_L^j A_\mu + \bar{u}_R^j N_{u,R}^\gamma \gamma^\mu u_R^j A_\mu + \bar{d}_R^j N_{d,R}^\gamma \gamma^\mu d_R^j A_\mu \\
& + \bar{l}_L^j N_L^\gamma \gamma^\mu l_L^j A_\mu + \bar{e}_R^j N_{e,R}^\gamma \gamma^\mu e_R^j A_\mu \\
& + \bar{l}_L^j N_{L,lep}^Z \gamma^\mu l_L^j Z_\mu + \bar{l}_L^j N_{L,lep}^{Z'} \gamma^\mu l_L^j Z'_\mu \\
& + \bar{e}_R^j N_{e,R}^Z \gamma^\mu e_R^j Z_\mu + \bar{e}_R^j N_{e,R}^{Z'} \gamma^\mu e_R^j Z'_\mu
\end{aligned} \tag{19}$$

where for the quarks we have

$$\begin{aligned}
N_L^{Z,j} &= -i \left(g \cos \theta_W T_3^L - g_Y \sin \theta_W \frac{\hat{Y}^L}{2} + g_z \varepsilon \frac{\hat{z}^L}{2} \right) \\
N_L^{Z',j} &= -i \left(-g \cos \theta_W T_3^L \varepsilon + g_Y \sin \theta_W \frac{\hat{Y}^L}{2} \varepsilon + g_z \frac{\hat{z}^L}{2} \right) \\
N_{u,R}^Z &= -i \left(-g_Y \sin \theta_W \frac{\hat{Y}^{u,R}}{2} + g_z \varepsilon \frac{\hat{z}^{u,R}}{2} \right) \\
N_{d,R}^Z &= -i \left(-g_Y \sin \theta_W \frac{\hat{Y}^{d,R}}{2} + g_z \varepsilon \frac{\hat{z}^{d,R}}{2} \right),
\end{aligned} \tag{20}$$

and similar expressions for the leptons. We rewrite the vector and the axial coupling of

the Z and Z' bosons to the quarks as

$$\begin{aligned}
\frac{-ig}{4c_w}\gamma^\mu g_V^{Z,j} &= \frac{-ig}{c_w}\frac{1}{2}\left[c_w^2 T_3^{L,j} - s_w^2\left(\frac{\hat{Y}_L^j}{2} + \frac{\hat{Y}_R^j}{2}\right) + \varepsilon\frac{g_z}{g}c_w\left(\frac{\hat{z}_{L,j}}{2} + \frac{\hat{z}_{R,j}}{2}\right)\right]\gamma^\mu \\
\frac{-ig}{4c_w}\gamma^\mu\gamma^5 g_A^{Z,j} &= \frac{-ig}{c_w}\frac{1}{2}\left[-c_w^2 T_3^{L,j} - s_w^2\left(\frac{\hat{Y}_R^j}{2} - \frac{\hat{Y}_L^j}{2}\right) + \varepsilon\frac{g_z}{g}c_w\left(\frac{\hat{z}_{R,j}}{2} - \frac{\hat{z}_{L,j}}{2}\right)\right]\gamma^\mu\gamma^5 \\
\frac{-ig}{4c_w}\gamma^\mu g_V^{Z',j} &= \frac{-ig}{c_w}\frac{1}{2}\left[-\varepsilon c_w^2 T_3^{L,j} + \varepsilon s_w^2\left(\frac{\hat{Y}_L^j}{2} + \frac{\hat{Y}_R^j}{2}\right) + \frac{g_z}{g}c_w\left(\frac{\hat{z}_{L,j}}{2} + \frac{\hat{z}_{R,j}}{2}\right)\right]\gamma^\mu \\
\frac{-ig}{4c_w}\gamma^\mu\gamma^5 g_A^{Z',j} &= \frac{-ig}{c_w}\frac{1}{2}\left[\varepsilon c_w^2 T_3^{L,j} + \varepsilon s_w^2\left(\frac{\hat{Y}_R^j}{2} - \frac{\hat{Y}_L^j}{2}\right) + \frac{g_z}{g}c_w\left(\frac{\hat{z}_{R,j}}{2} - \frac{\hat{z}_{L,j}}{2}\right)\right]\gamma^\mu\gamma^5,
\end{aligned} \tag{21}$$

where j is an index which represents the quark or the lepton and we have set $\sin\theta_W = s_w$, $\cos\theta_W = c_w$ for brevity.

The decay rates into leptons for the Z and the Z' are universal and are given by

$$\begin{aligned}
\Gamma(\mathcal{Z} \rightarrow l\bar{l}) &= \frac{g^2}{192\pi c_w^2} M_{\mathcal{Z}} \left[(g_V^{\mathcal{Z},l})^2 + (g_A^{\mathcal{Z},l})^2 \right] = \frac{\alpha_{em}}{48s_w^2 c_w^2} M_{\mathcal{Z}} \left[(g_V^{\mathcal{Z},l})^2 + (g_A^{\mathcal{Z},l})^2 \right], \\
\Gamma(\mathcal{Z} \rightarrow \psi_i \bar{\psi}_i) &= \frac{N_c \alpha_{em}}{48s_w^2 c_w^2} M_{\mathcal{Z}} \left[(g_V^{\mathcal{Z},\psi_i})^2 + (g_A^{\mathcal{Z},\psi_i})^2 \right] \times \\
&\quad \left[1 + \frac{\alpha_s(M_{\mathcal{Z}})}{\pi} + 1.409 \frac{\alpha_s^2(M_{\mathcal{Z}})}{\pi^2} - 12.77 \frac{\alpha_s^3(M_{\mathcal{Z}})}{\pi^3} \right],
\end{aligned} \tag{22}$$

where $i = u, d, c, s$ and $\mathcal{Z} = Z, Z'$.

For the Z' and Z decays into heavy quarks we obtain

$$\begin{aligned}
\Gamma(\mathcal{Z} \rightarrow b\bar{b}) &= \frac{N_c \alpha_{em}}{48s_w^2 c_w^2} M_{\mathcal{Z}} \left[(g_V^{\mathcal{Z},b})^2 + (g_A^{\mathcal{Z},b})^2 \right] \times \\
&\quad \left[1 + \frac{\alpha_s(M_{\mathcal{Z}})}{\pi} + 1.409 \frac{\alpha_s^2(M_{\mathcal{Z}})}{\pi^2} - 12.77 \frac{\alpha_s^3(M_{\mathcal{Z}})}{\pi^3} \right], \\
\Gamma(\mathcal{Z} \rightarrow t\bar{t}) &= \frac{N_c \alpha_{em}}{48s_w^2 c_w^2} M_{\mathcal{Z}} \sqrt{1 - 4\frac{m_t^2}{M_{\mathcal{Z}}^2}} \times \\
&\quad \left[(g_V^{\mathcal{Z},t})^2 \left(1 + 2\frac{m_t^2}{M_{\mathcal{Z}}^2} \right) + (g_A^{\mathcal{Z},t})^2 \left(1 - 4\frac{m_t^2}{M_{\mathcal{Z}}^2} \right) \right] \times \\
&\quad \left[1 + \frac{\alpha_s(M_{\mathcal{Z}})}{\pi} + 1.409 \frac{\alpha_s^2(M_{\mathcal{Z}})}{\pi^2} - 12.77 \frac{\alpha_s^3(M_{\mathcal{Z}})}{\pi^3} \right].
\end{aligned} \tag{23}$$

The total hadronic widths are defined by

$$\Gamma_Z \equiv \Gamma(Z \rightarrow \text{hadrons}) = \sum_i \Gamma(Z \rightarrow \psi_i \bar{\psi}_i)$$

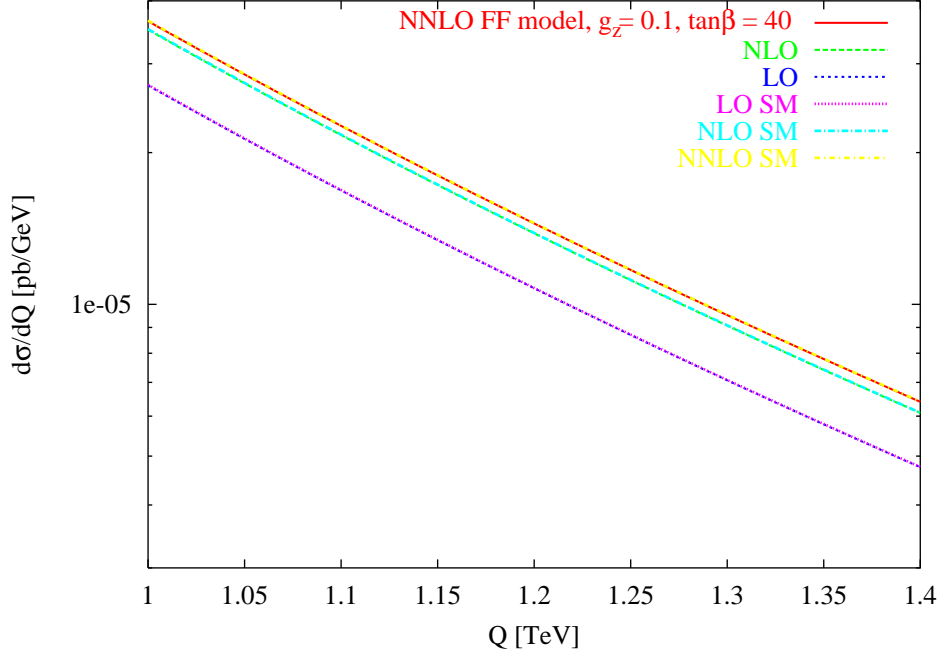


Figure 2: Plot of the LO, NLO and NNLO cross section for the free fermionic model with $M_{Z'} = 800$ GeV in the TeVs region.

$$\Gamma_{Z'} \equiv \Gamma(Z' \rightarrow \text{hadrons}) = \sum_i \Gamma(Z' \rightarrow \psi_i \bar{\psi}_i) \quad (24)$$

where we refer to hadrons not containing bottom and top quarks (i.e. $i = u, d, c, s$). We also ignore electroweak corrections and all fermion masses with the exception of the top-quark mass, while we have included the relevant QCD corrections. Similarly to [10] we have considered only tree level decays into fermions, assuming that the decays into particles other than the SM fermions are either invisible or are negligible in their branching ratios, then the total decay rate for the Z and Z' is given by

$$\begin{aligned} \Gamma_Z &= \sum_{i=u,d,c,s} \Gamma(Z \rightarrow \psi_i \bar{\psi}_i) + \Gamma(Z \rightarrow b\bar{b}) + 3\Gamma(Z \rightarrow l\bar{l}) + 3\Gamma(Z \rightarrow \nu_l \bar{\nu}_l) \\ \Gamma_{Z'} &= \sum_{i=u,d,c,s} \Gamma(Z' \rightarrow \psi_i \bar{\psi}_i) + \Gamma(Z' \rightarrow b\bar{b}) + \Gamma(Z' \rightarrow t\bar{t}) + 3\Gamma(Z' \rightarrow l\bar{l}) + 3\Gamma(Z' \rightarrow \nu_l \bar{\nu}_l). \end{aligned} \quad (25)$$

We also recall that the point-like cross sections for the photon, the SM Z_0 and the new Z' gauge boson are written as

$$\begin{aligned} \sigma_\gamma(Q^2) &= \frac{4\pi\alpha_{em}^2}{3Q^4} \frac{1}{N_c} \\ \sigma_Z(Q^2, M_Z^2) &= \frac{\pi\alpha_{em}}{4M_Z \sin^2 \theta_W \cos^2 \theta_W N_c} \frac{\Gamma_{Z \rightarrow \bar{l}l}}{(Q^2 - M_Z^2)^2 + M_Z^2 \Gamma_Z^2} \end{aligned}$$

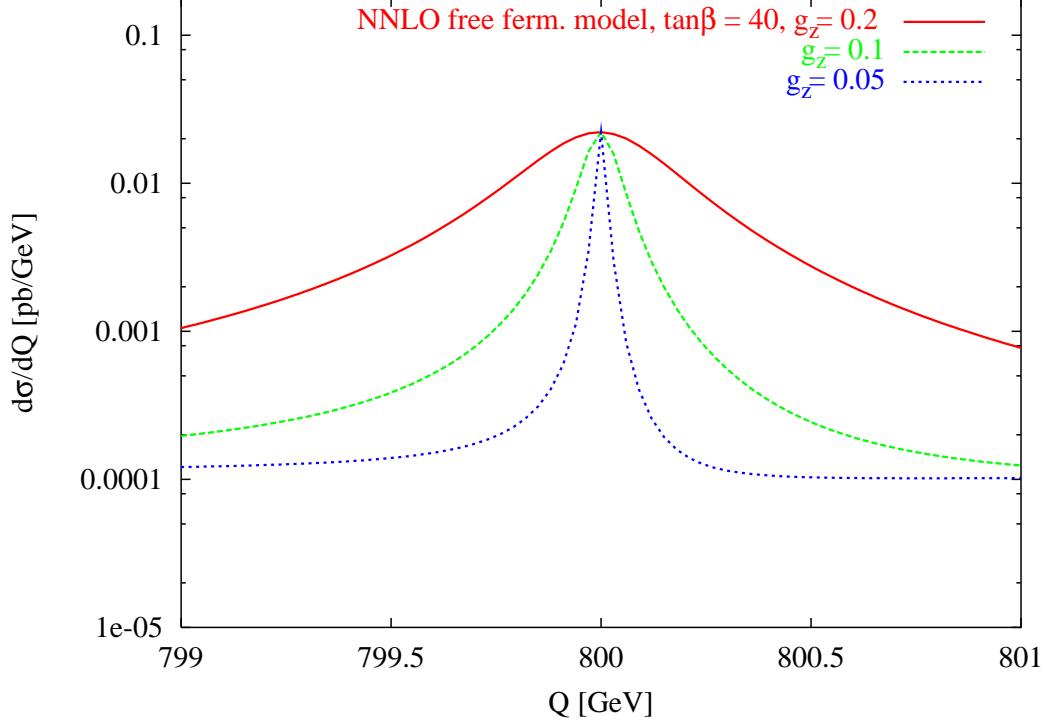


Figure 3: Free fermionic model at the LHC, $\tan\beta = 40$

$$\sigma_{Z,\gamma}(Q^2, M_Z^2) = \frac{\pi\alpha_{em}^2 (1 - 4\sin^2\theta_W)}{6 \sin^2\theta_W \cos^2\theta_W} \frac{(Q^2 - M_Z^2)}{N_C Q^2 (Q^2 - M_Z^2)^2 + M_Z^2 \Gamma_Z^2}, \quad (26)$$

where N_C is the number of colours, and

$$\begin{aligned} \sigma_{Z'}(Q^2) &= \frac{\pi\alpha_{em}}{4M_{Z'} \sin^2\theta_W \cos^2\theta_W N_c} \frac{\Gamma_{Z' \rightarrow \bar{l}l}}{(Q^2 - M_{Z'}^2)^2 + M_{Z'}^2 \Gamma_{Z'}^2}, \\ \sigma_{Z',\gamma}(Q^2) &= \frac{\pi\alpha_{em}^2}{6N_c \sin^2\theta_W \cos^2\theta_W} \frac{g_V^{Z',l} g_V^{\gamma,l} (Q^2 - M_{Z'}^2)}{Q^2 (Q^2 - M_{Z'}^2)^2 + M_{Z'}^2 \Gamma_{Z'}^2}, \\ \sigma_{Z',Z}(Q^2) &= \frac{\pi\alpha_{em}^2}{96} \frac{[g_V^{Z',l} g_V^{Z,l} + g_A^{Z',l} g_A^{Z,l}]}{\sin^4\theta_W \cos^4\theta_W N_c} \frac{(Q^2 - M_Z^2)(Q^2 - M_{Z'}^2) + M_Z \Gamma_Z M_{Z'} \Gamma_{Z'}}{[(Q^2 - M_{Z'}^2)^2 + M_{Z'}^2 \Gamma_{Z'}^2][(Q^2 - M_Z^2)^2 + M_Z^2 \Gamma_Z^2]}. \end{aligned} \quad (27)$$

The contributions such as Z, γ and similar denote the interference terms. At LO (or leading order) the process proceeds through the $q\bar{q}$ annihilation channel and is $O(1)$ in the strong coupling constant α_s . The NLO (or next-to-leading order) corrections involve virtual corrections with one gluon exchanged in the initial state and real emissions involving a single gluon, which is integrated over phase space. These corrections are $O(\alpha_s)$ in the strong coupling. The change induced by moving from LO to NLO amounts to approximately a 20 to 30 % in the numerical value of the cross section that we consider. At

the highest accuracy, we use in our analysis partonic contributions with hard scattering computed at NNLO, or $O(\alpha_s^2)$. At this order typical real emissions involve 2 partons in the final state - which are integrated over their phase space- and two-loop virtual corrections at the same perturbative order. The cross section for the invariant mass distributions factorizes at a perturbative level in terms of a NNLO (next-to-next-to-leading, or $O(\alpha_s^2)$) contribution W_V (which takes into account all the initial state emissions of real gluons and all the virtual corrections) and a point-like cross section. The computation of W_V can be found in [11] to which we refer for more details. A similar factorization holds also for the total cross section if we use the narrow width approximation. At NLO (next-to-leading order, or $O(\alpha_s)$). The colour-averaged inclusive differential cross section for the reaction $p + p \rightarrow l_1 + l_2 + X$, is given by

$$\frac{d\sigma}{dQ^2} = \tau \sigma_V(Q^2, M_V^2) W_V(\tau, Q^2) \quad \tau = \frac{Q^2}{S}, \quad (28)$$

where all the hadronic initial state information is contained in the hadronic structure function which is defined as

$$W_V(\tau, Q^2) = \sum_{i,j} \int_0^1 dx_1 \int_0^1 dx_2 \int_0^1 dx \delta(\tau - xx_1x_2) PD_{i,j}^V(x_1, x_2, \mu_F^2) \Delta_{i,j}(x, Q^2, \mu_F^2), \quad (29)$$

where the quantity $PD_{i,j}^V(x_1, x_2, \mu_F^2)$ contains all the information about the parton distribution functions and their evolution up to the μ_F^2 scale, while the functions $\Delta_{i,j}(x, Q^2, \mu_F^2)$ are the hard scatterings. This factorization formula is universal for invariant mass distributions mediated by s-channel exchanges of neutral or charged currents. The hard scatterings can be expanded in a series in terms of the running coupling constant $\alpha_s(\mu_R^2)$ as

$$\Delta_{i,j}(x, Q^2, \mu_F^2) = \sum_{n=0}^{\infty} \alpha_s^n(\mu_R^2) \Delta_{i,j}^{(n)}(x, Q^2, \mu_F, \mu_R^2). \quad (30)$$

In principle, factorization and renormalization scales should be kept separate in order to determine the overall scale dependence of the results. However, as we are going to show, the high-end of the Drell-Yan distribution is not so sensitive to these higher order corrections, at least for the models that we have studied.

4 Numerical Results

In our analysis we have decided to compare our results with a series of models introduced in [10]. We refer to this work for more details concerning their general origin. We just

mention that the construction of models with extra Z' using a bottom-up approach is, in general, rather straightforward, being based mostly on the principle of cancellation of the gauge cubic $U(1)_{Z'}^3$ and mixed anomalies. One of the most economical ways to proceed is to introduce just one additional $SU(2)_W$ Higgs doublet and an extra scalar (weak) singlet, as in [12], and one right-handed neutrino per generation in order to generate reasonable operators for their Majorana and Dirac masses. However, more general solutions of the anomaly equations are possible by enlarging the fermion spectrum and/or enlarging the scalar sector [13]. In [10] the scalar sector is enlarged with 2 Higgs doublets and one (weak) scalar singlet.

Anomalous constructions, instead, require a different approach and several phenomenological analysis have been presented recently [14, 15, 16, 17] that try to identify the signature of these peculiar realizations. In the anomalous models, due to the absence of the non-resonant behaviour of the s-channel (at least in the double prompt photon production), the chiral anomaly induces a unitarity growth which should be present in correlated studies of other channels [17]. For non anomalous Z' the phenomenological predictions are, as we are going to show, rather similar for all the models - at least in the mass invariant distributions in Drell-Yan - and the possibility to identify the underlying interaction requires a careful study of the forward-backward and/or charge asymmetries [18]. This is not going to be an easy task at the LHC, given the size of the cross section at the tail of the invariant mass distribution, the rather narrow widths, and given the presence of both theoretical and experimental errors in the parton distributions (pdf's), unless the gauge coupling is quite sizeable ($O(1)$). We refer to [19] for an accurate analysis of the experimental errors on the pdf's in the case of the Z peak. It has been shown that the errors on the pdf's are comparable with the overall reduction of the cross section as we move from the NLO to the NNLO.

These source of ambiguities, known as experimental errors, unfortunately do not take into consideration the theoretical errors due to the implementation of the solution of the DGLAP in the evolution codes, which amount to a theoretical uncertainty [20]. Once all these sources of indeterminations are combined together, the expected error on the Z peak is likely to be much larger than 3 %. Given the large amount of data that will accumulate in the first runs (for $Q = M_Z$), which will soon reduce the statistical errors on the measurements far below the 0.1 % value, there will be severe issues to be addressed also from the theoretical side in order to match this far larger experimental accuracy. The possibility to use determinations of the pdf's on the Z peak for further studies of the Z' resonances at larger invariant mass values of the lepton pair, have to face several additional issues, such as the presence of an additional scale, which is $Q = M_{Z'}$, new respect to the $Q = M_Z$ scale used as a benchmark for partonometry in the first accelerator runs. We

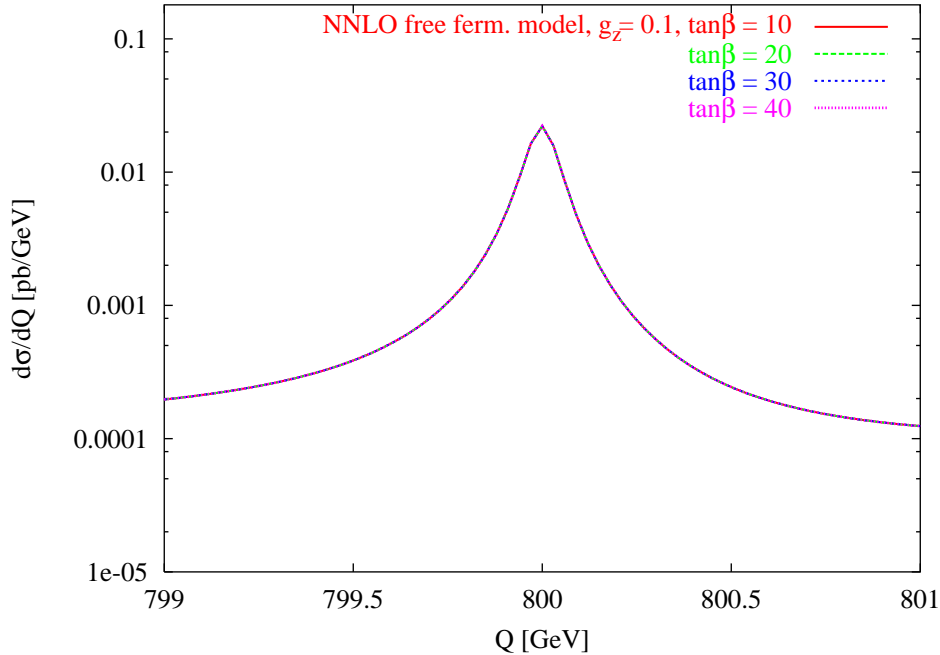


Figure 4: Free fermionic model at the LHC, $g_z = 0.1$

remind that logarithms of these two scales may also play a role especially if $M_{Z'}$ is far larger than M_Z . With these words of caution in mind we proceed with our exploration of the class of models that we have selected, starting from the string model and then analyzing the bottom-up models mentioned above [10]. These are studied in the limit $z_{H_1} = z_{H_2} = 0$, with the mass of the extra Z' generated only by the extra singlet scalar ϕ . In the string model, as one can see from (9), only the two Higgses H_U and H_D contribute to the mass of the new gauge boson. The differences between these two types of models are, however, not relevant for this analysis, since the mass of the extra gauge boson is essentially a free parameter in both cases.

The set of pdf's that we have used for our analysis is MRST2001 [21], which is given in parametric form, evolved with CANDIA (see [22]). The models analyzed numerically are the free fermionic one, “F”, discussed in the previous sections, and the “ $B - L$ ”, “ $q + u$ ”, “ $10 + \bar{5}$ ” and “ $d-u$ ”, using the notations of [10].

Our results are organized in a series of plots on the various resonances and in some tables which are useful in order to pin down the actual numerical value of the various cross sections at a given invariant mass.

4.1 $M_{Z'} = 0.8 \text{ TeV}$

We show in Fig. 1 a plot of the Z' resonance around a typical value of 800 GeV for the FF model and the SM. The coupling of the extra neutral gauge boson is taken to be 0.05, with $\tan\beta = 10$. We remark that the dependence of the resonance on this second parameter is negligible. In fact the relevant parameters are the coupling constant g_Z and the mass $M_{Z'}$. Notice that the width is very narrow ($\approx 1 \text{ GeV}$) and basically invisible in an experimental analysis. Nevertheless it is, at least theoretically, useful to try to characterize the signal and the background even in this (and other similar) not favourable cases.

Assuming an integrated luminosity of $100fb^{-1}/y$ after the first 3 years at the LHC (per experiment), we would expect 10 background events versus a signal of approximately 30 events. Notice that LO, NLO and NNLO determinations are, essentially, coincident for all the practical purposes.

In Fig. 2 we show the tail of the distribution for a run with $M_{Z'} = 800 \text{ GeV}$, where we have just modified $\tan\beta$ and we have increased the coupling to $g_Z = 0.1$. For Q around 1.2 TeV the determinations of the cross section in the FF and SM models are basically overlapping as we move from LO to NLO and NNLO. The LO determination in the SM moves up toward the FF result as we increase the perturbative order. Also in this case, given the small size of the cross section ($\approx 10^{-2} \text{ fb}$) the possibility to resolve these differences experimentally is remote. In Fig. 3 we vary the coupling constants of the extra $U(1)$ from a very small value $g_Z = 0.05$ up to $g_Z = 0.2$. The only variation in the result is due to the width that increases from 1 to approximately 3-4 GeV's. Here we have chosen $\tan\beta = 40$, and, as shown in Fig. 4 there is essentially no variation on the shape of the resonance due to this variable. In Figs. 5 and 6 we perform a comparative study of all the models and the SM background for a resonance mass of 800 GeV. There are only minor differences between the 4 bottom-up models and the FF model. The FF model shows a resonance curve which sits in the middle of all the determinations but is, for the rest, overlapping with the other curves. The “ $B - L$ ” model, in all the cases, shows a wider width among all, with the “ $q + u$ ” model quite similar to it. The “ $d - u$ ” model has the narrowest width. This feature is particularly obvious from Fig. 7 where the result is numerically smoothed out by the increased value of the coupling, which is now doubled compared to Fig. 6.

4.2 $M_{Z'} = 1.2 \text{ TeV}$

We illustrate in the next 3 figures our results for the various models for $M_{Z'} = 1.2 \text{ TeV}$. Fig. 8 shows the behaviour of the cross section for this new mass value with $g_Z = 0.1$,

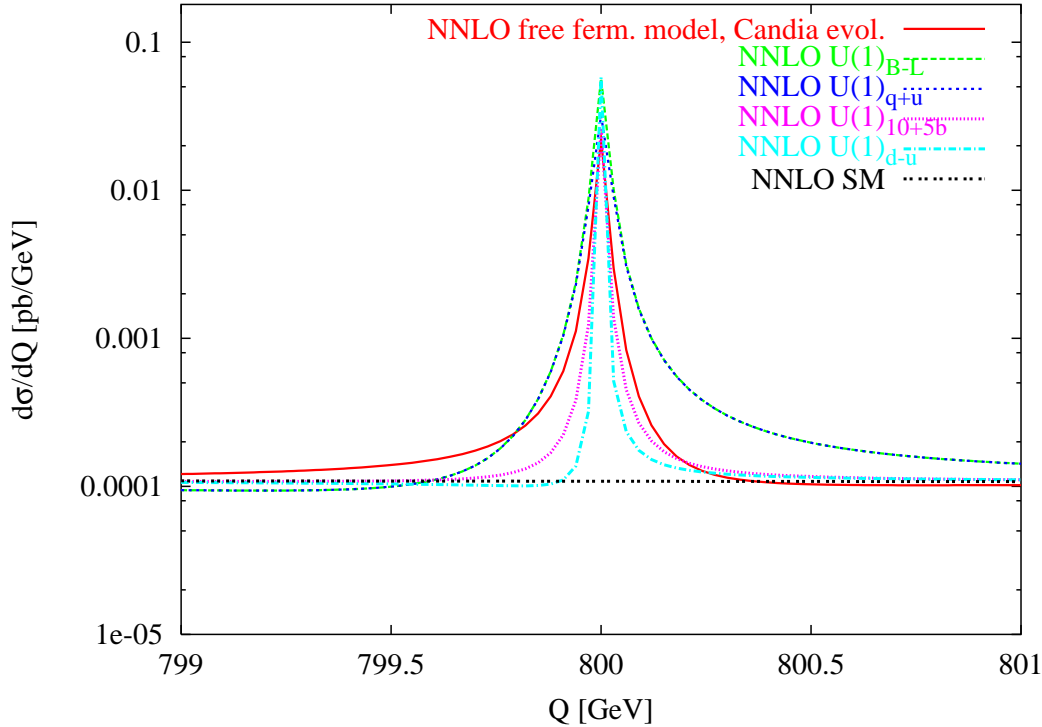


Figure 5: Free fermionic model at the LHC, $\tan\beta = 40$ and $g_z = 0.05$

and the corresponding result for the SM case. The QCD corrections are very small and it is likely that the only role of these corrections, at these large Q values, is to stabilize the dependence of the perturbative series from the factorization/renormalization scales. In our case we have chosen, for simplicity $\mu_F = \mu_R = Q$, where μ_R and μ_F are the renormalization and factorization scale, respectively. The separation of this dependence can be done as in [20], by relating the coupling constants at the two scales (μ_F, μ_R) .

This separation, in general, needs to be done both in the hard scattering and in the evolution. A zoom of the resonance region is shown in Fig. 9, which shows that the reduction of the signal is by a factor of 10 compared to the case of $M_{Z'} = 0.8$ TeV. This drastic reduction of the cross section is one of the reason why the search of extra neutral currents, if these are mediated by new gauge bosons of mass above the 1 TeV range, may take several years of LHC luminosity to be performed, unless the new gauge coupling is larger. As shown in Fig. 10, as we move away from the resonance region, the SM background and the FF result overlap. An interesting feature is that the K-factors for the SM result are much larger than for the FF case, especially as we move from LO to NLO. At NNLO both curves, however, overlap.

We show, in Fig. 11 a plot of the shape of the resonance region for $M_{Z'} = 2.5$ TeV. The width is very narrow (2 GeV) and the size of the cross section down by a factor of 100

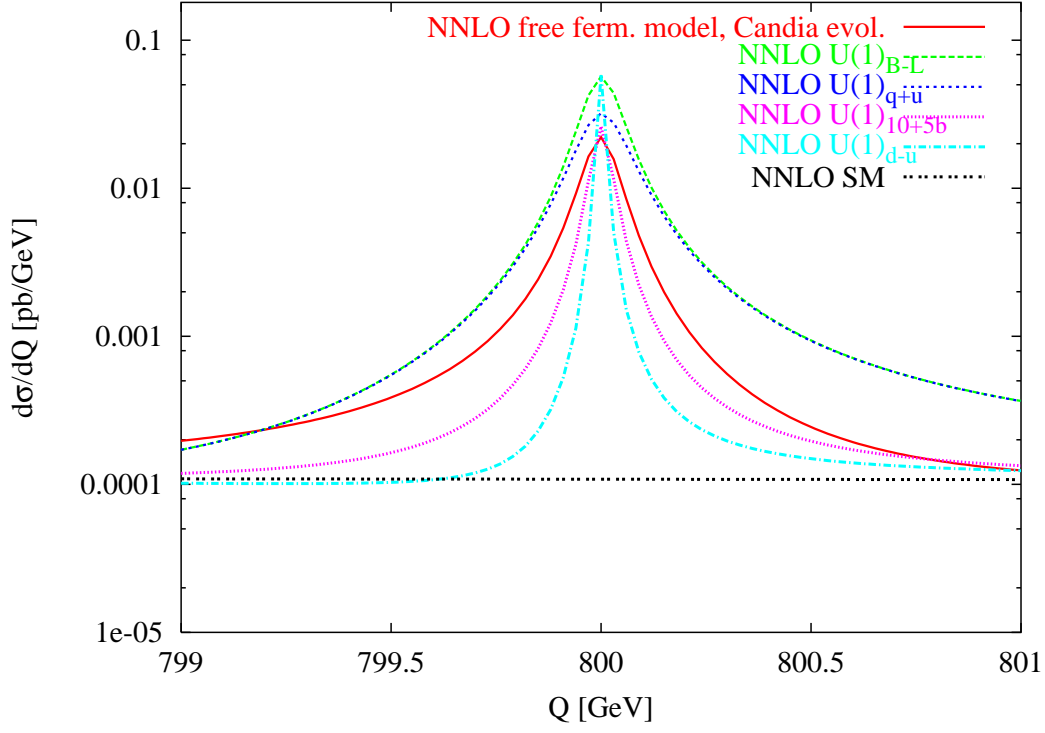


Figure 6: Free fermionic model at the LHC, $\tan\beta = 40$ and $g_z = 0.1$

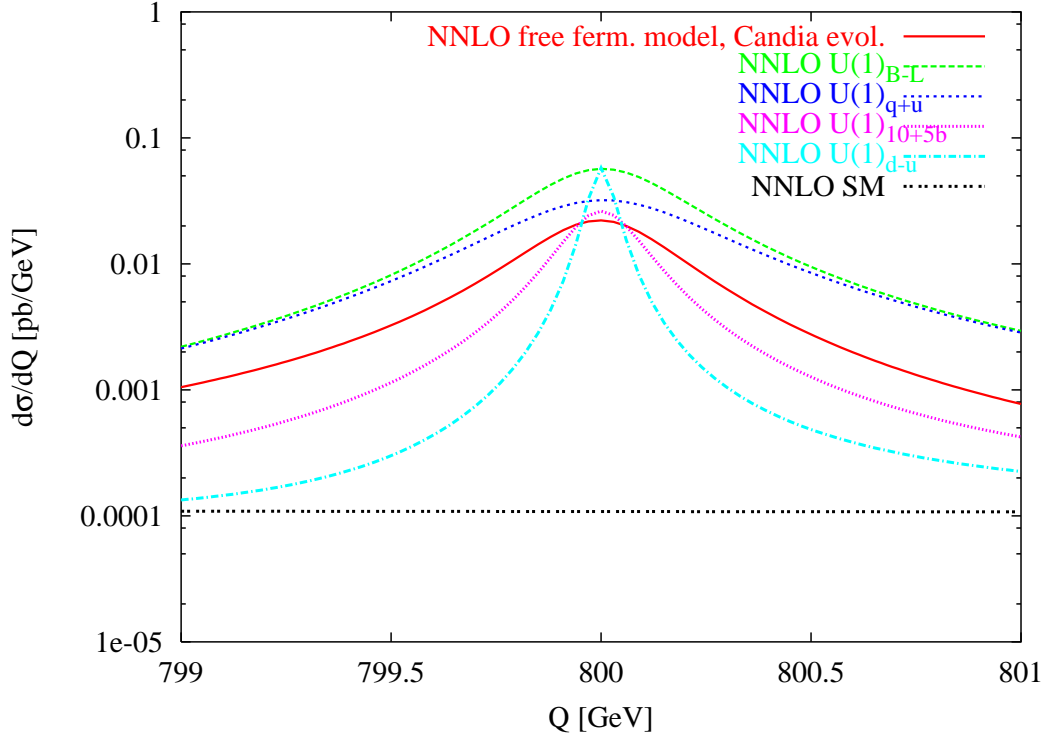


Figure 7: Free fermionic model at the LHC, $\tan\beta = 40$ and $g_z = 0.2$

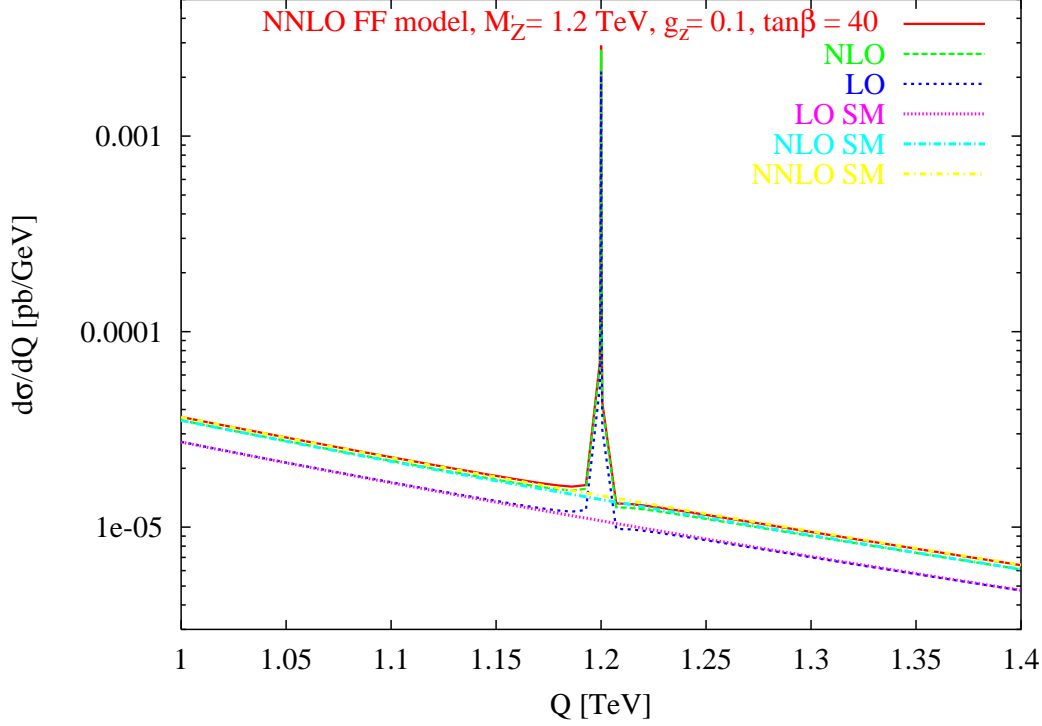


Figure 8: Free fermionic model at the LHC, $\tan\beta = 40$ and $g_z = 0.1$

compared to the case of $M_{Z'} = 1.2$ TeV. A similar analysis of the shapes of the resonances is shown in Fig. 12 where we have chosen but this time we have varied the strength of the new coupling in order to show the widening of the width, which may ease the detection of the new neutral currents. As shown in Tab. (1), only at large values of the couplings the size of the width is such to ensure a more direct identification of the resonance, which should probably be around 30 GeV or more, in order not to be missed. We conclude this section with the discussion of some results concerning the study of the variation of the cross section $d\sigma/dQ(Q = M_{Z'})$ (on the peak) as we vary the factorization scale. In Fig. 13 the scale μ_f has been varied in the interval $1/2M_{Z'} < \mu_f < 2M_{Z'}$ for a mass $M_{Z'} = 600$ GeV. These variations are rather small over all the energy interval that we have analyzed and show consistently the reduction of the scale dependence of the result moving from LO to NLO and NNLO. The cross section is sizeable in particular above the 4 TeV scale, especially for larger couplings, although the presence of the resonance is not resolved in this figure given the small width. Finally, in Fig. 14 we plot the total cross section as a function of the energy for 3 values of the new gauge couplings for $M_{Z'}=1.2$ TeV. Also in this case the rise of the cross section gets sizeable for larger value of the couplings.

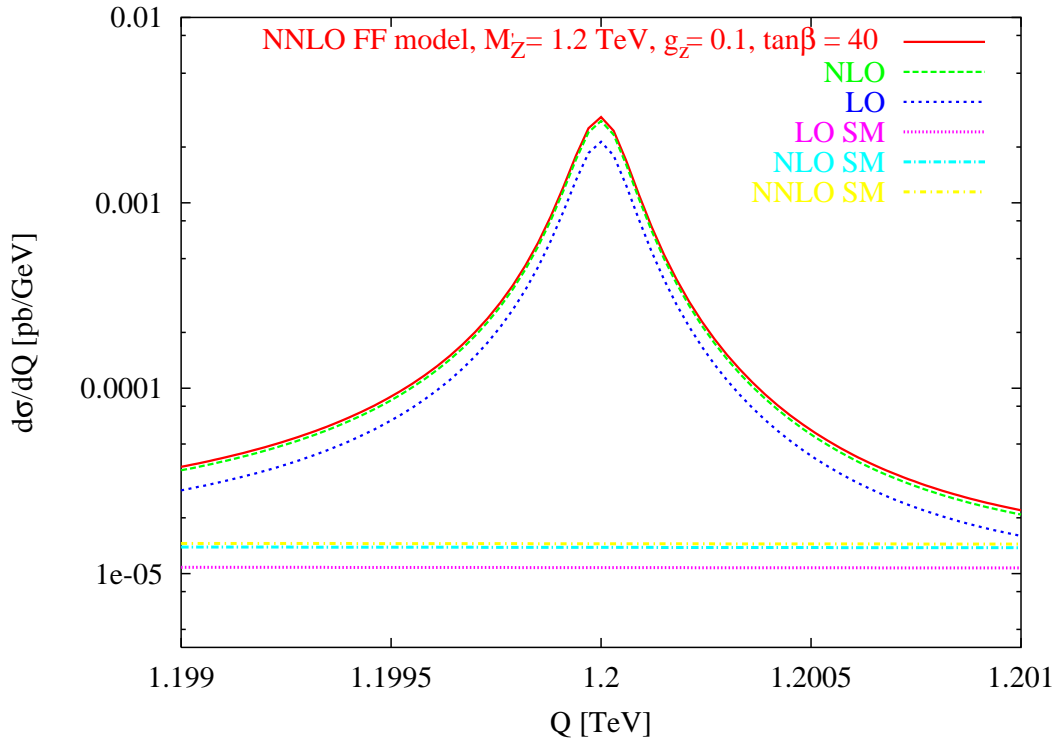


Figure 9: Free fermionic model at the LHC, $\tan\beta = 40$ and $g_z = 0.1$. Shown are also the SM results through the same perturbative orders.

4.3 NLO/NNLO comparisons and relative differences

We have included a set of tables which may be useful for actual experimental searches and comparisons. In table 2 we show the LO and in table 3 the NLO results for the invariant mass distributions for the first choice (800 GeV) of the mass of the extra Z' in all the models, and the corresponding value also for the SM. In all the cases the proximity among the various determinations is quite evident, except on the resonance, where the values show a wide variability. The pattern at NNLO, shown in table 4 is similar, and the changes in the cross sections from NLO to NNLO in most of the cases are around 3 % or less. These changes are of the same order of those obtained by a study of the K-factors in the case of the Z resonance [20]. Also for this kinematical region, as on the Z peak [20], the changes from LO to NLO are around 20-30 %, and cover the bulk of the QCD corrections. The last several tables describe the relative differences between the results of the various models and the SM, normalized to the SM values, at the various perturbative orders and for 3 values of the coupling constants $g_z = 0.05, 0.1$ and 0.2 . They give an indication of the role played by the changes in the coupling on the behaviour of these observables at the tails of the resonance region. In tables 5 and 6 the region that we explore is between 1 and 1.5 TeV. It is rather clear from these results that for a weakly

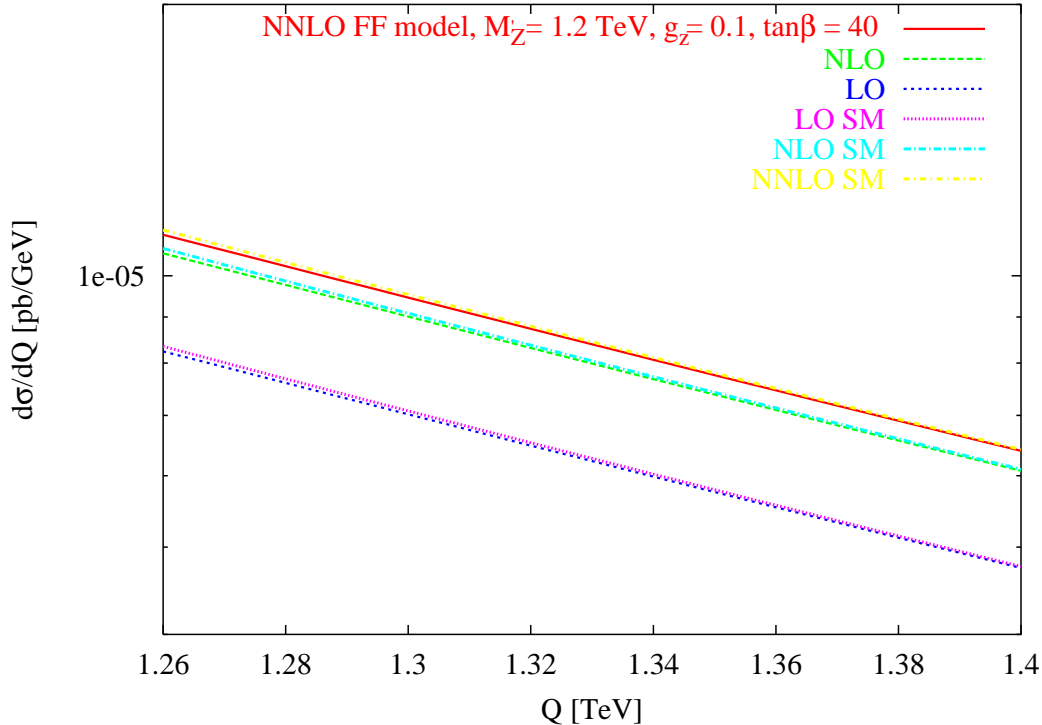


Figure 10: Free fermionic model at the LHC, $\tan\beta = 40$ and $g_z = 0.1$ and the corresponding SM results. The plot is a zooming of the resonance shape shown in Fig. 8

coupled Z' ($g_z = 0.05$) the NLO and NNLO variations respect to the SM result are essentially similar. The differences at NLO between the various models and the NLO SM are a fraction of a percent. Therefore, NNLO QCD corrections will not help in this region for such weakly coupled extra Z' . The differences are not more sizeable as we increase the new gauge coupling to 0.1, as shown in 7 and 8. Both at NLO and NNLO the difference between the SM background and all the other models is smaller than 1 %. Things are not much better for a value of the coupling constant equal to 0.2. The differences between the SM and various models in this region of fast fall-off can be of the order of only 2 %, and just for one model (“ $B - L$ ”). Given also the small size of these cross sections, which are of the order of 3×10^{-2} fb, it is hard to separate the various contributions. Naturally, the situation will improve considerably if we allow a larger gauge coupling since the differences between signal and background can become, in principle, quite large.

5 Conclusions

We performed a preliminary comparative analysis of the behaviour of several models containing extra neutral currents in anomaly-free constructions and we discussed the

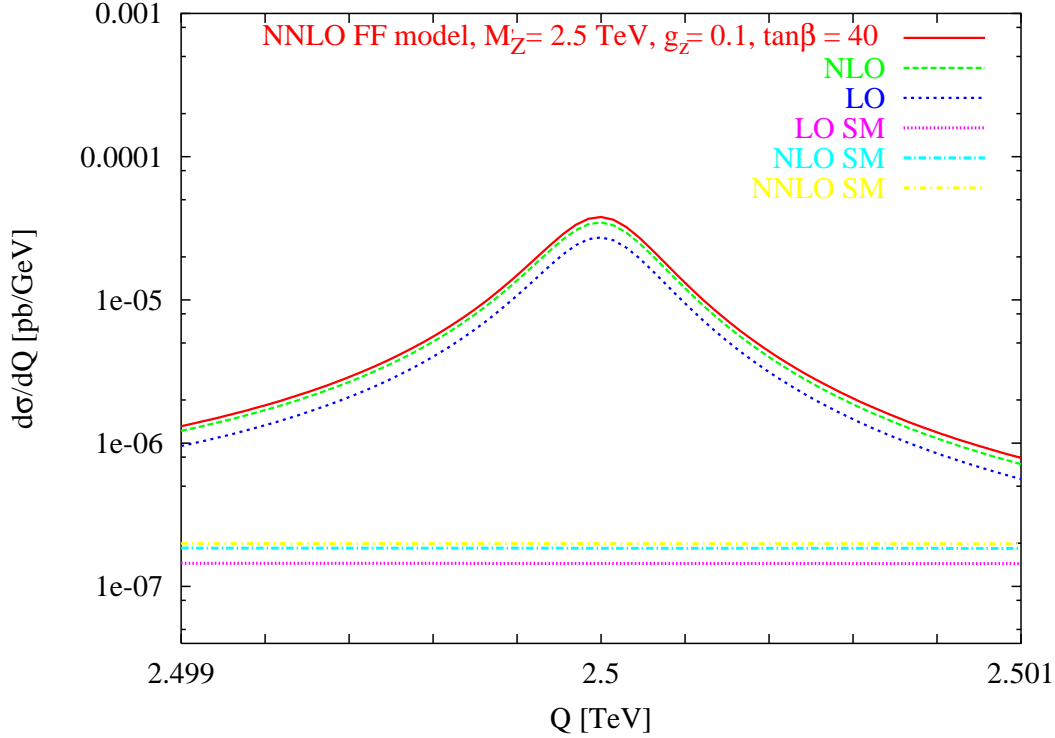


Figure 11: Free fermionic model and the corresponding SM results at all the three orders for $M_{Z'} = 2.5$ TeV.

implications of the results for actual experimental searches at the LHC. Compared to other studies, our objective has been to compare signal and QCD background in a series of models, with the highest accuracy, which can be systematically performed through NNLO. As expected, the critical parameters in order to be able to see a signal of these new interactions at the new collider are the size of the gauge coupling and the mass of the extra gauge boson, while the specific charge assignments of the models play a minor role. Other parameters such as $\tan\beta$ also do not play any significant role in these types of searches. It is reasonable to believe that much of the potentiality for discovering the new resonance, if found, is its width, and all the models analyzed so far show very similar patterns, with a gauging of “ $B - L$ ” being the one that has a slightly wider resonant behaviour. Being the coupling so important in order to identify which model has better chances to be confirmed or ruled out, it is necessary, especially in bottom-up constructions, to rely on more precise investigations of possible scenarios for the running of the couplings, which are not addressed in approaches of these types. In the case of the free fermionic $U(1)$ that we have analyzed, the possibility to include these models in a more general scenario is natural, since they are naturally produced by a unification scheme, but is left for future studies. On the other hand, in these and similar models obtained either in the string picture or in Grand Unification, the decoupling of part of the “extra stuff” that would

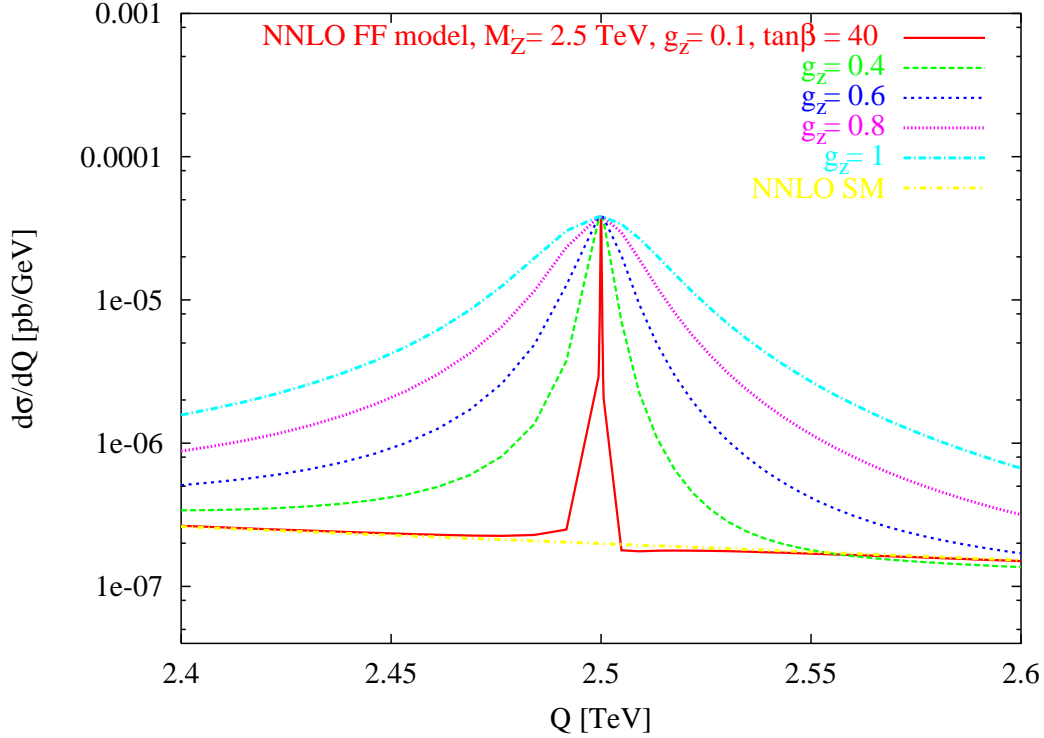


Figure 12: Free fermionic model and the corresponding SM results at NNLO for $M_{Z'} = 2.5$ TeV for different values of g_z larger than $g_z = 0.1$.

complicate the scenario that we have analyzed, requires extra assumptions, which would also affect the running of the couplings of the extra $U(1)$'s. These assumptions would introduce various alternatives on the choice of the symmetry breaking scales, threshold enhancements, and so on, which amount, however, to important phenomenological details which strongly affect this search.

Since the V-A structure of the couplings exhibits differences with respect to other Z' models a measurement of forward-backward asymmetries and/or of charge asymmetries could be helpful [18], but only if the gauge coupling is sizeable. The discrimination among the various models remains a very difficult issue for which NNLO QCD determinations, at least in leptonproduction, though useful, do not seem to be necessary in a first analysis. For those values of the mass of the extra Z' that we have considered these corrections cannot be isolated, while the NLO effects remain important.

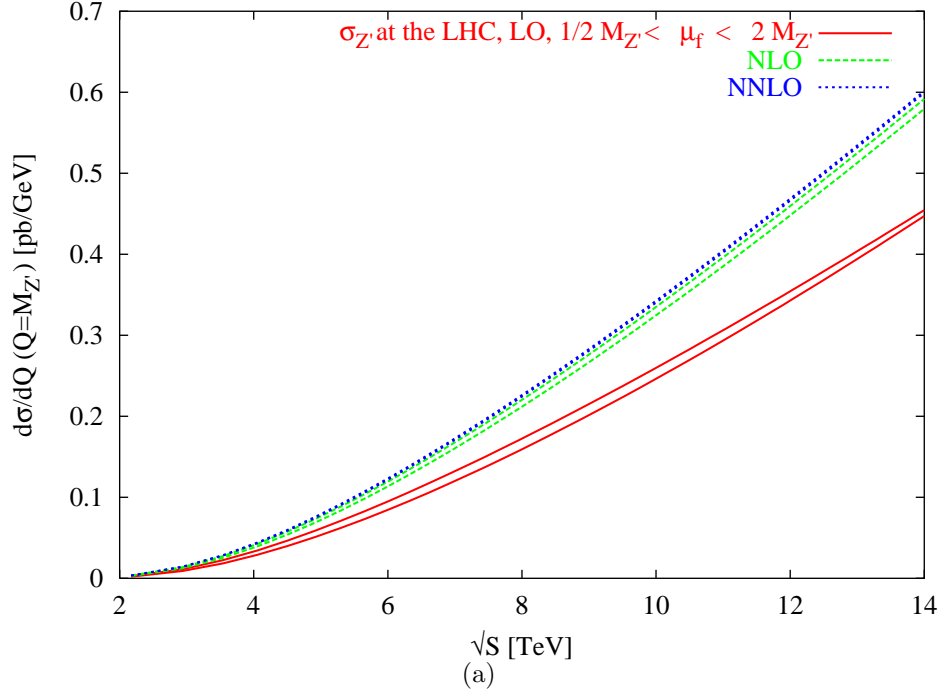


Figure 13: Study of the μ_F scale dependence in the total cross section for the $U(1)_{B-L}$ model with $M_{Z'} = 0.6$ TeV and $g_z = 0.1$. Here we have chosen $M_{Z'} = Q$ for simplicity.

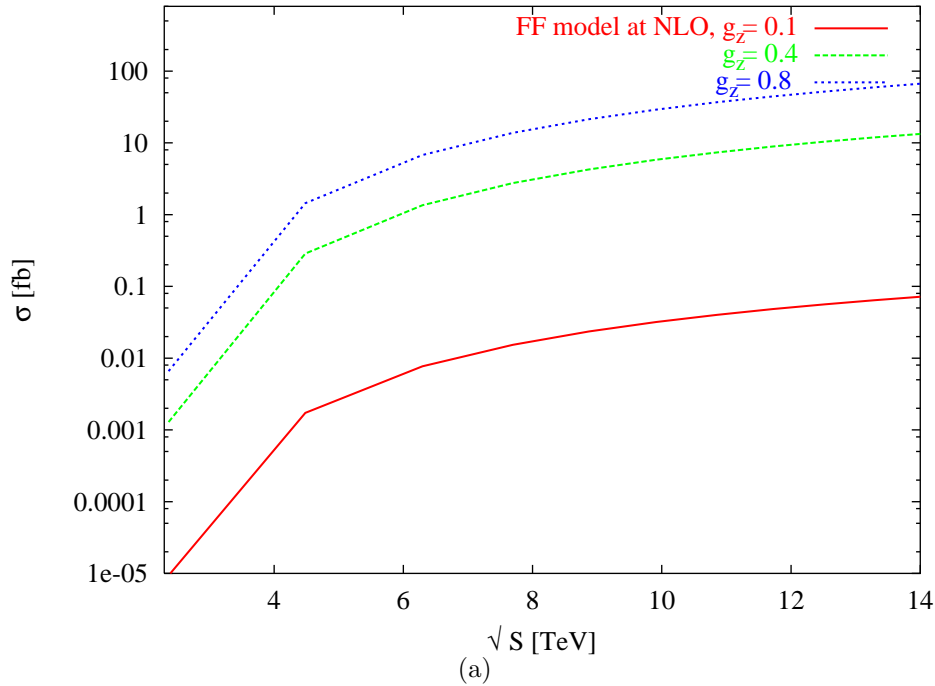


Figure 14: Total cross section for the Free fermionic model at NLO for three different values of g_z and for $M_{Z'} = 1.2$ TeV. Here we have chosen $\mu_F = \mu_R = Q$ for simplicity and we have integrated the mass invariant distribution on the interval $M_{Z'} \pm 3\Gamma_{Z'}$.

$\Gamma_{M_{Z'}}(g_z)$ [GeV]			
g_z	$M_{Z'} = 0.8$ TeV	$M_{Z'} = 1.2$ TeV	$M_{Z'} = 2.5$ TeV
0.02	0.004	0.005	0.012
0.05	0.024	0.036	0.075
0.1	0.097	0.146	0.303
0.2	0.388	0.584	1.215
0.3	0.875	1.314	2.735
0.4	1.555	2.336	4.863
0.5	2.430	3.650	7.598
0.6	3.500	5.256	10.94
0.7	4.764	7.154	14.89
0.8	6.223	9.344	19.45
0.9	7.876	11.82	24.61
1	9.723	14.60	30.39

Table 1: Dependence of the total width on the coupling constant g_z for the free fermionic model with $M_{Z'} = 800$ GeV, $M_{Z'} = 1.2$ TeV and $M_{Z'} = 2.5$ TeV.

Acknowledgements

We thank Simone Morelli for discussions and for various cross-checks in the numerical analysis. M.G. thanks the Theory Division at the University of Liverpool for hospitality and the Royal Society for financial support. The work of C.C. was supported (in part) by the European Union through the Marie Curie Research and Training Network “Universenet” (MRTN-CT-2006-035863) and by The Interreg II Crete-Cyprus Program. He thanks the Theory group at Crete for hospitality. The work of A.E.F. is supported in part the STFC.

$d\sigma_{LO}/dQ$ [pb/GeV], $M'_Z = 800$, $g_z = 0.1$, $\tan\beta = 40$, Candia evol.						
Q [GeV]	$\sigma_{LO}(Q)$ FFM	$\sigma_{LO}(Q)$ $U(1)_{B-L}$	$\sigma_{LO}(Q)$ $U(1)_{q+u}$	$\sigma_{LO}(Q)$ $U(1)_{10+5}$	$\sigma_{LO}(Q)$ $U(1)_{d-u}$	$\sigma_{LO}(SM)$
750	$1.1101 \cdot 10^{-4}$	$1.0854 \cdot 10^{-4}$	$1.0854 \cdot 10^{-4}$	$1.1017 \cdot 10^{-4}$	$1.1011 \cdot 10^{-4}$	$1.1033 \cdot 10^{-4}$
761	$1.0355 \cdot 10^{-4}$	$1.0050 \cdot 10^{-4}$	$1.0050 \cdot 10^{-4}$	$1.0250 \cdot 10^{-4}$	$1.0243 \cdot 10^{-4}$	$1.0269 \cdot 10^{-4}$
773	$9.6852 \cdot 10^{-5}$	$9.2759 \cdot 10^{-5}$	$9.2759 \cdot 10^{-5}$	$9.5421 \cdot 10^{-5}$	$9.5315 \cdot 10^{-5}$	$9.5674 \cdot 10^{-5}$
784	$9.1225 \cdot 10^{-5}$	$8.4635 \cdot 10^{-5}$	$8.4635 \cdot 10^{-5}$	$8.8822 \cdot 10^{-5}$	$8.8633 \cdot 10^{-5}$	$8.9212 \cdot 10^{-5}$
796	$9.1654 \cdot 10^{-5}$	$7.2110 \cdot 10^{-5}$	$7.2111 \cdot 10^{-5}$	$8.2428 \cdot 10^{-5}$	$8.1409 \cdot 10^{-5}$	$8.3259 \cdot 10^{-5}$
800	$1.6448 \cdot 10^{-2}$	$4.2388 \cdot 10^{-2}$	$2.3928 \cdot 10^{-2}$	$1.9570 \cdot 10^{-2}$	$4.3085 \cdot 10^{-2}$	$8.1086 \cdot 10^{-5}$
800	$4.9572 \cdot 10^{-4}$	$1.9334 \cdot 10^{-3}$	$1.8812 \cdot 10^{-3}$	$2.8631 \cdot 10^{-4}$	$1.5888 \cdot 10^{-4}$	$8.0955 \cdot 10^{-5}$
801	$1.7452 \cdot 10^{-4}$	$6.8269 \cdot 10^{-4}$	$6.7771 \cdot 10^{-4}$	$1.4480 \cdot 10^{-4}$	$1.1071 \cdot 10^{-4}$	$8.0839 \cdot 10^{-5}$
839	$6.4010 \cdot 10^{-5}$	$6.6355 \cdot 10^{-5}$	$6.6355 \cdot 10^{-5}$	$6.4761 \cdot 10^{-5}$	$6.4800 \cdot 10^{-5}$	$6.4607 \cdot 10^{-5}$
868	$5.4301 \cdot 10^{-5}$	$5.5480 \cdot 10^{-5}$	$5.5480 \cdot 10^{-5}$	$5.4686 \cdot 10^{-5}$	$5.4706 \cdot 10^{-5}$	$5.4610 \cdot 10^{-5}$
900	$4.5656 \cdot 10^{-5}$	$4.6371 \cdot 10^{-5}$	$4.6371 \cdot 10^{-5}$	$4.5892 \cdot 10^{-5}$	$4.5904 \cdot 10^{-5}$	$4.5847 \cdot 10^{-5}$

Table 2: LO invariant mass distributions

$d\sigma_{NLO}/dQ$ [pb/GeV], $M'_Z = 800$, $g_z = 0.1$, $\tan\beta = 40$, Candia evol.						
Q [GeV]	$\sigma_{NLO}(Q)$ FFM	$\sigma_{NLO}(Q)$ $U(1)_{B-L}$	$\sigma_{NLO}(Q)$ $U(1)_{q+u}$	$\sigma_{NLO}(Q)$ $U(1)_{10+5}$	$\sigma_{NLO}(Q)$ $U(1)_{d-u}$	$\sigma_{NLO}(SM)$
750	$1.4362 \cdot 10^{-4}$	$1.4048 \cdot 10^{-4}$	$1.4048 \cdot 10^{-4}$	$1.4257 \cdot 10^{-4}$	$1.4248 \cdot 10^{-4}$	$1.4276 \cdot 10^{-4}$
761	$1.3394 \cdot 10^{-4}$	$1.3008 \cdot 10^{-4}$	$1.3008 \cdot 10^{-4}$	$1.3263 \cdot 10^{-4}$	$1.3252 \cdot 10^{-4}$	$1.3287 \cdot 10^{-4}$
773	$1.2526 \cdot 10^{-4}$	$1.2006 \cdot 10^{-4}$	$1.2006 \cdot 10^{-4}$	$1.2346 \cdot 10^{-4}$	$1.2331 \cdot 10^{-4}$	$1.2377 \cdot 10^{-4}$
784	$1.1794 \cdot 10^{-4}$	$1.0958 \cdot 10^{-4}$	$1.0958 \cdot 10^{-4}$	$1.1492 \cdot 10^{-4}$	$1.1465 \cdot 10^{-4}$	$1.1540 \cdot 10^{-4}$
796	$1.1834 \cdot 10^{-4}$	$9.3647 \cdot 10^{-5}$	$9.3648 \cdot 10^{-5}$	$1.0671 \cdot 10^{-4}$	$1.0530 \cdot 10^{-4}$	$1.0769 \cdot 10^{-4}$
800	$2.1411 \cdot 10^{-2}$	$5.4992 \cdot 10^{-2}$	$3.1043 \cdot 10^{-2}$	$2.5389 \cdot 10^{-2}$	$5.5896 \cdot 10^{-2}$	$1.0487 \cdot 10^{-4}$
800	$6.4893 \cdot 10^{-4}$	$2.5014 \cdot 10^{-3}$	$2.4339 \cdot 10^{-3}$	$3.6947 \cdot 10^{-4}$	$2.0566 \cdot 10^{-4}$	$1.0470 \cdot 10^{-4}$
801	$2.2882 \cdot 10^{-4}$	$8.8180 \cdot 10^{-4}$	$8.7537 \cdot 10^{-4}$	$1.8666 \cdot 10^{-4}$	$1.4323 \cdot 10^{-4}$	$1.0455 \cdot 10^{-4}$
839	$8.2772 \cdot 10^{-5}$	$8.5749 \cdot 10^{-5}$	$8.5749 \cdot 10^{-5}$	$8.3712 \cdot 10^{-5}$	$8.3771 \cdot 10^{-5}$	$8.3523 \cdot 10^{-5}$
868	$7.0183 \cdot 10^{-5}$	$7.1679 \cdot 10^{-5}$	$7.1679 \cdot 10^{-5}$	$7.0666 \cdot 10^{-5}$	$7.0696 \cdot 10^{-5}$	$7.0573 \cdot 10^{-5}$
900	$5.8982 \cdot 10^{-5}$	$5.9888 \cdot 10^{-5}$	$5.9888 \cdot 10^{-5}$	$5.9278 \cdot 10^{-5}$	$5.9296 \cdot 10^{-5}$	$5.9222 \cdot 10^{-5}$

Table 3: NLO distributions for $750 < Q < 900$ GeV

$d\sigma_{NNLO}/dQ$ [pb/GeV], $M'_Z = 800$, $g_z = 0.1$, $\tan\beta = 40$, Candia evol.						
Q [GeV]	$\sigma_{NNLO}(Q)$ FFM	$\sigma_{NNLO}(Q)$ $U(1)_{B-L}$	$\sigma_{NNLO}(Q)$ $U(1)_{q+u}$	$\sigma_{NNLO}(Q)$ $U(1)_{10+5}$	$\sigma_{NNLO}(Q)$ $U(1)_{d-u}$	$\sigma_{NNLO}(SM)$
750	$1.4793 \cdot 10^{-4}$	$1.4472 \cdot 10^{-4}$	$1.4472 \cdot 10^{-4}$	$1.4686 \cdot 10^{-4}$	$1.4676 \cdot 10^{-4}$	$1.4705 \cdot 10^{-4}$
761	$1.3803 \cdot 10^{-4}$	$1.3407 \cdot 10^{-4}$	$1.3407 \cdot 10^{-4}$	$1.3669 \cdot 10^{-4}$	$1.3657 \cdot 10^{-4}$	$1.3693 \cdot 10^{-4}$
773	$1.2914 \cdot 10^{-4}$	$1.2382 \cdot 10^{-4}$	$1.2382 \cdot 10^{-4}$	$1.2730 \cdot 10^{-4}$	$1.2714 \cdot 10^{-4}$	$1.2762 \cdot 10^{-4}$
784	$1.2164 \cdot 10^{-4}$	$1.1308 \cdot 10^{-4}$	$1.1308 \cdot 10^{-4}$	$1.1856 \cdot 10^{-4}$	$1.1827 \cdot 10^{-4}$	$1.1904 \cdot 10^{-4}$
796	$1.2207 \cdot 10^{-4}$	$9.6772 \cdot 10^{-5}$	$9.6773 \cdot 10^{-5}$	$1.1017 \cdot 10^{-4}$	$1.0867 \cdot 10^{-4}$	$1.1114 \cdot 10^{-4}$
800	$2.2140 \cdot 10^{-2}$	$5.6805 \cdot 10^{-2}$	$3.2066 \cdot 10^{-2}$	$2.6233 \cdot 10^{-2}$	$5.7755 \cdot 10^{-2}$	$1.0825 \cdot 10^{-4}$
800	$6.7222 \cdot 10^{-4}$	$2.5818 \cdot 10^{-3}$	$2.5121 \cdot 10^{-3}$	$3.8114 \cdot 10^{-4}$	$2.1235 \cdot 10^{-4}$	$1.0808 \cdot 10^{-4}$
801	$2.3717 \cdot 10^{-4}$	$9.0971 \cdot 10^{-4}$	$9.0307 \cdot 10^{-4}$	$1.9249 \cdot 10^{-4}$	$1.4787 \cdot 10^{-4}$	$1.0793 \cdot 10^{-4}$
839	$8.5581 \cdot 10^{-5}$	$8.8638 \cdot 10^{-5}$	$8.8638 \cdot 10^{-5}$	$8.6542 \cdot 10^{-5}$	$8.6606 \cdot 10^{-5}$	$8.6349 \cdot 10^{-5}$
868	$7.2645 \cdot 10^{-5}$	$7.4182 \cdot 10^{-5}$	$7.4182 \cdot 10^{-5}$	$7.3139 \cdot 10^{-5}$	$7.3171 \cdot 10^{-5}$	$7.3044 \cdot 10^{-5}$
900	$6.1122 \cdot 10^{-5}$	$6.2054 \cdot 10^{-5}$	$6.2054 \cdot 10^{-5}$	$6.1425 \cdot 10^{-5}$	$6.1444 \cdot 10^{-5}$	$6.1368 \cdot 10^{-5}$

Table 4: NNLO distributions for $750 < Q < 900$ GeV

$ \sigma_{nlo}^{SM} - \sigma_{nlo}^i /\sigma_{nlo}^{SM}\%$, $M'_Z = 800$, $g_z = 0.05$, $\tan\beta = 40$, Candia evol.						
Q [GeV]	$\sigma_{nlo}^{SM}(Q)$ [pb/GeV]	$\Delta_{nlo}^{FFM}\%$	$\Delta_{nlo}^{B-L}\%$	$\Delta_{nlo}^{q+u}\%$	$\Delta_{nlo}^{10+5}\%$	$\Delta_{nlo}^{d-u}\%$
1000	$3.5146 \cdot 10^{-5}$	$6.5325 \cdot 10^{-2}$	$1.6003 \cdot 10^{-1}$	$1.6003 \cdot 10^{-1}$	$1.0162 \cdot 10^{-2}$	$1.4126 \cdot 10^{-2}$
1015	$3.2618 \cdot 10^{-5}$	$6.2528 \cdot 10^{-2}$	$1.5220 \cdot 10^{-1}$	$1.5220 \cdot 10^{-1}$	$9.5155 \cdot 10^{-3}$	$1.3203 \cdot 10^{-2}$
1030	$3.0299 \cdot 10^{-5}$	$6.0105 \cdot 10^{-2}$	$1.4541 \cdot 10^{-1}$	$1.4541 \cdot 10^{-1}$	$8.9574 \cdot 10^{-3}$	$1.2402 \cdot 10^{-2}$
1045	$2.8168 \cdot 10^{-5}$	$5.7987 \cdot 10^{-2}$	$1.3947 \cdot 10^{-1}$	$1.3947 \cdot 10^{-1}$	$8.4716 \cdot 10^{-3}$	$1.1701 \cdot 10^{-2}$
1060	$2.6209 \cdot 10^{-5}$	$5.6121 \cdot 10^{-2}$	$1.3424 \cdot 10^{-1}$	$1.3424 \cdot 10^{-1}$	$8.0455 \cdot 10^{-3}$	$1.1083 \cdot 10^{-2}$
1165	$1.6156 \cdot 10^{-5}$	$4.7509 \cdot 10^{-2}$	$1.1003 \cdot 10^{-1}$	$1.1003 \cdot 10^{-1}$	$6.1091 \cdot 10^{-3}$	$8.2061 \cdot 10^{-3}$
1210	$1.3265 \cdot 10^{-5}$	$4.5240 \cdot 10^{-2}$	$1.0361 \cdot 10^{-1}$	$1.0361 \cdot 10^{-1}$	$5.6126 \cdot 10^{-3}$	$7.4369 \cdot 10^{-3}$
1250	$1.1183 \cdot 10^{-5}$	$4.3636 \cdot 10^{-2}$	$9.9050 \cdot 10^{-2}$	$9.9050 \cdot 10^{-2}$	$5.2687 \cdot 10^{-3}$	$6.8881 \cdot 10^{-3}$
1355	$7.2763 \cdot 10^{-6}$	$4.0639 \cdot 10^{-2}$	$9.0453 \cdot 10^{-2}$	$9.0453 \cdot 10^{-2}$	$4.6479 \cdot 10^{-3}$	$5.8404 \cdot 10^{-3}$
1425	$5.5361 \cdot 10^{-6}$	$3.9279 \cdot 10^{-2}$	$8.6492 \cdot 10^{-2}$	$8.6492 \cdot 10^{-2}$	$4.3830 \cdot 10^{-3}$	$5.3492 \cdot 10^{-3}$
1500	$4.1734 \cdot 10^{-6}$	$3.8186 \cdot 10^{-2}$	$8.3253 \cdot 10^{-2}$	$8.3253 \cdot 10^{-2}$	$4.1841 \cdot 10^{-3}$	$4.9401 \cdot 10^{-3}$

Table 5: Percentage differences at NLO. We define $\Delta_{nlo}^i = |\sigma_{nlo}^{SM} - \sigma_{nlo}^i|/\sigma_{nlo}^{SM}$ where $i = FFM, B - L, q + u, 10 + \bar{5}, d - u$.

$ \sigma_{nnlo}^{SM} - \sigma_{nnlo}^i /\sigma_{nnlo}^{SM}\%$, $M'_Z = 800$, $g_z = 0.05$, $\tan\beta = 40$, Candia evol.						
Q [GeV]	$\sigma_{nnlo}^{SM}(Q)$ [pb/GeV]	$\Delta_{nnlo}^{FFM}\%$	$\Delta_{nnlo}^{B-L}\%$	$\Delta_{nnlo}^{q+u}\%$	$\Delta_{nnlo}^{10+5}\%$	$\Delta_{nnlo}^{d-u}\%$
1000	$3.6546 \cdot 10^{-5}$	$6.4565 \cdot 10^{-2}$	$1.5879 \cdot 10^{-1}$	$1.5879 \cdot 10^{-1}$	$9.8298 \cdot 10^{-3}$	$1.4114 \cdot 10^{-2}$
1015	$3.3935 \cdot 10^{-5}$	$6.1789 \cdot 10^{-2}$	$1.5099 \cdot 10^{-1}$	$1.5099 \cdot 10^{-1}$	$9.1914 \cdot 10^{-3}$	$1.3191 \cdot 10^{-2}$
1030	$3.1537 \cdot 10^{-5}$	$5.9383 \cdot 10^{-2}$	$1.4423 \cdot 10^{-1}$	$1.4423 \cdot 10^{-1}$	$8.6399 \cdot 10^{-3}$	$1.2390 \cdot 10^{-2}$
1045	$2.9334 \cdot 10^{-5}$	$5.7279 \cdot 10^{-2}$	$1.3831 \cdot 10^{-1}$	$1.3831 \cdot 10^{-1}$	$8.1595 \cdot 10^{-3}$	$1.1689 \cdot 10^{-2}$
1060	$2.7306 \cdot 10^{-5}$	$5.5425 \cdot 10^{-2}$	$1.3310 \cdot 10^{-1}$	$1.3310 \cdot 10^{-1}$	$7.7381 \cdot 10^{-3}$	$1.1071 \cdot 10^{-2}$
1165	$1.6888 \cdot 10^{-5}$	$4.6857 \cdot 10^{-2}$	$1.0895 \cdot 10^{-1}$	$1.0895 \cdot 10^{-1}$	$5.8167 \cdot 10^{-3}$	$8.1924 \cdot 10^{-3}$
1210	$1.3884 \cdot 10^{-5}$	$4.4594 \cdot 10^{-2}$	$1.0254 \cdot 10^{-1}$	$1.0254 \cdot 10^{-1}$	$5.3213 \cdot 10^{-3}$	$7.4223 \cdot 10^{-3}$
1250	$1.1718 \cdot 10^{-5}$	$4.2991 \cdot 10^{-2}$	$9.7986 \cdot 10^{-2}$	$9.7986 \cdot 10^{-2}$	$4.9768 \cdot 10^{-3}$	$6.8729 \cdot 10^{-3}$
1355	$7.6472 \cdot 10^{-6}$	$3.9988 \cdot 10^{-2}$	$8.9375 \cdot 10^{-2}$	$8.9375 \cdot 10^{-2}$	$4.3502 \cdot 10^{-3}$	$5.8236 \cdot 10^{-3}$
1425	$5.8293 \cdot 10^{-6}$	$3.8618 \cdot 10^{-2}$	$8.5395 \cdot 10^{-2}$	$8.5395 \cdot 10^{-2}$	$4.0792 \cdot 10^{-3}$	$5.3312 \cdot 10^{-3}$
1500	$4.4031 \cdot 10^{-6}$	$3.7510 \cdot 10^{-2}$	$8.2129 \cdot 10^{-2}$	$8.2129 \cdot 10^{-2}$	$3.8720 \cdot 10^{-3}$	$4.9211 \cdot 10^{-3}$

Table 6: Percentage differences at NNLO. We define $\Delta_{nnlo}^i = |\sigma_{nnlo}^{SM} - \sigma_{nnlo}^i|/\sigma_{nnlo}^{SM}$.

$ \sigma_{nlo}^{SM} - \sigma_{nlo}^i /\sigma_{nlo}^{SM}\%$, $M'_Z = 800$, $g_z = 0.1$, $\tan\beta = 40$, Candia evol.						
Q [GeV]	$\sigma_{nlo}^{SM}(Q)$ [pb/GeV]	$\Delta_{nlo}^{FFM}\%$	$\Delta_{nlo}^{B-L}\%$	$\Delta_{nlo}^{q+u}\%$	$\Delta_{nlo}^{10+5}\%$	$\Delta_{nlo}^{d-u}\%$
1000	$3.5146 \cdot 10^{-5}$	$2.4555 \cdot 10^{-1}$	$6.5950 \cdot 10^{-1}$	$6.5950 \cdot 10^{-1}$	$5.5268 \cdot 10^{-2}$	$7.0677 \cdot 10^{-2}$
1015	$3.2618 \cdot 10^{-5}$	$2.3454 \cdot 10^{-1}$	$6.2764 \cdot 10^{-1}$	$6.2764 \cdot 10^{-1}$	$5.2612 \cdot 10^{-2}$	$6.6957 \cdot 10^{-2}$
1030	$3.0299 \cdot 10^{-5}$	$2.2500 \cdot 10^{-1}$	$6.0005 \cdot 10^{-1}$	$6.0005 \cdot 10^{-1}$	$5.0320 \cdot 10^{-2}$	$6.3730 \cdot 10^{-2}$
1045	$2.8168 \cdot 10^{-5}$	$2.1666 \cdot 10^{-1}$	$5.7593 \cdot 10^{-1}$	$5.7593 \cdot 10^{-1}$	$4.8324 \cdot 10^{-2}$	$6.0904 \cdot 10^{-2}$
1060	$2.6209 \cdot 10^{-5}$	$2.0931 \cdot 10^{-1}$	$5.5469 \cdot 10^{-1}$	$5.5469 \cdot 10^{-1}$	$4.6574 \cdot 10^{-2}$	$5.8410 \cdot 10^{-2}$
1165	$1.6156 \cdot 10^{-5}$	$1.7534 \cdot 10^{-1}$	$4.5649 \cdot 10^{-1}$	$4.5649 \cdot 10^{-1}$	$3.8610 \cdot 10^{-2}$	$4.6791 \cdot 10^{-2}$
1210	$1.3265 \cdot 10^{-5}$	$1.6639 \cdot 10^{-1}$	$4.3048 \cdot 10^{-1}$	$4.3048 \cdot 10^{-1}$	$3.6562 \cdot 10^{-2}$	$4.3677 \cdot 10^{-2}$
1250	$1.1183 \cdot 10^{-5}$	$1.6007 \cdot 10^{-1}$	$4.1202 \cdot 10^{-1}$	$4.1202 \cdot 10^{-1}$	$3.5137 \cdot 10^{-2}$	$4.1449 \cdot 10^{-2}$
1355	$7.2763 \cdot 10^{-6}$	$1.4826 \cdot 10^{-1}$	$3.7722 \cdot 10^{-1}$	$3.7722 \cdot 10^{-1}$	$3.2554 \cdot 10^{-2}$	$3.7189 \cdot 10^{-2}$
1425	$5.5361 \cdot 10^{-6}$	$1.4291 \cdot 10^{-1}$	$3.6118 \cdot 10^{-1}$	$3.6118 \cdot 10^{-1}$	$3.1440 \cdot 10^{-2}$	$3.5182 \cdot 10^{-2}$
1500	$4.1734 \cdot 10^{-6}$	$1.3861 \cdot 10^{-1}$	$3.4806 \cdot 10^{-1}$	$3.4806 \cdot 10^{-1}$	$3.0591 \cdot 10^{-2}$	$3.3504 \cdot 10^{-2}$

Table 7: Percentage differences at NLO for $g_z = 0.1$. Here and in the following we use the same notation of the previous tables.

30

$ \sigma_{nnlo}^{SM} - \sigma_{nnlo}^i /\sigma_{nnlo}^{SM}\%$, $M'_Z = 800$, $g_z = 0.1$, $\tan\beta = 40$, Candia evol.						
Q [GeV]	$\sigma_{nnlo}^{SM}(Q)$ [pb/GeV]	$\Delta_{nnlo}^{FFM}\%$	$\Delta_{nnlo}^{B-L}\%$	$\Delta_{nnlo}^{q+u}\%$	$\Delta_{nnlo}^{10+5}\%$	$\Delta_{nnlo}^{d-u}\%$
1000	$3.6546 \cdot 10^{-5}$	$2.4248 \cdot 10^{-1}$	$6.5458 \cdot 10^{-1}$	$6.5458 \cdot 10^{-1}$	$5.3970 \cdot 10^{-2}$	$7.0662 \cdot 10^{-2}$
1015	$3.3935 \cdot 10^{-5}$	$2.3155 \cdot 10^{-1}$	$6.2284 \cdot 10^{-1}$	$6.2284 \cdot 10^{-1}$	$5.1346 \cdot 10^{-2}$	$6.6942 \cdot 10^{-2}$
1030	$3.1537 \cdot 10^{-5}$	$2.2208 \cdot 10^{-1}$	$5.9536 \cdot 10^{-1}$	$5.9536 \cdot 10^{-1}$	$4.9081 \cdot 10^{-2}$	$6.3715 \cdot 10^{-2}$
1045	$2.9334 \cdot 10^{-5}$	$2.1379 \cdot 10^{-1}$	$5.7133 \cdot 10^{-1}$	$5.7133 \cdot 10^{-1}$	$4.7108 \cdot 10^{-2}$	$6.0888 \cdot 10^{-2}$
1060	$2.7306 \cdot 10^{-5}$	$2.0649 \cdot 10^{-1}$	$5.5017 \cdot 10^{-1}$	$5.5017 \cdot 10^{-1}$	$4.5376 \cdot 10^{-2}$	$5.8394 \cdot 10^{-2}$
1165	$1.6888 \cdot 10^{-5}$	$1.7269 \cdot 10^{-1}$	$4.5223 \cdot 10^{-1}$	$4.5223 \cdot 10^{-1}$	$3.7478 \cdot 10^{-2}$	$4.6774 \cdot 10^{-2}$
1210	$1.3884 \cdot 10^{-5}$	$1.6377 \cdot 10^{-1}$	$4.2627 \cdot 10^{-1}$	$4.2627 \cdot 10^{-1}$	$3.5438 \cdot 10^{-2}$	$4.3659 \cdot 10^{-2}$
1250	$1.1718 \cdot 10^{-5}$	$1.5744 \cdot 10^{-1}$	$4.0781 \cdot 10^{-1}$	$4.0781 \cdot 10^{-1}$	$3.4013 \cdot 10^{-2}$	$4.1431 \cdot 10^{-2}$
1355	$7.6472 \cdot 10^{-6}$	$1.4560 \cdot 10^{-1}$	$3.7296 \cdot 10^{-1}$	$3.7296 \cdot 10^{-1}$	$3.1411 \cdot 10^{-2}$	$3.7169 \cdot 10^{-2}$
1425	$5.8293 \cdot 10^{-6}$	$1.4021 \cdot 10^{-1}$	$3.5685 \cdot 10^{-1}$	$3.5685 \cdot 10^{-1}$	$3.0275 \cdot 10^{-2}$	$3.5160 \cdot 10^{-2}$
1500	$4.4031 \cdot 10^{-6}$	$1.3585 \cdot 10^{-1}$	$3.4362 \cdot 10^{-1}$	$3.4362 \cdot 10^{-1}$	$2.9397 \cdot 10^{-2}$	$3.3481 \cdot 10^{-2}$

Table 8: Percentage differences at NNLO for $g_z = 0.1$

$ \sigma_{nlo}^{SM} - \sigma_{nlo}^i /\sigma_{nlo}^{SM}\%$, $M'_Z = 800$, $g_z = 0.2$, $\tan\beta = 40$, Candia evol.						
Q [GeV]	$\sigma_{nlo}^{SM}(Q)$ [pb/GeV]	$\Delta_{nlo}^{FFM}\%$	$\Delta_{nlo}^{B-L}\%$	$\Delta_{nlo}^{q+u}\%$	$\Delta_{nlo}^{10+5}\%$	$\Delta_{nlo}^{d-u}\%$
1000	$3.5146 \cdot 10^{-5}$	$9.4061 \cdot 10^{-1}$	$2.7377 \cdot 10^{+0}$	$2.7377 \cdot 10^{+0}$	$2.4462 \cdot 10^{-1}$	$2.9911 \cdot 10^{-1}$
1015	$3.2618 \cdot 10^{-5}$	$8.9927 \cdot 10^{-1}$	$2.6020 \cdot 10^{+0}$	$2.6020 \cdot 10^{+0}$	$2.3306 \cdot 10^{-1}$	$2.8399 \cdot 10^{-1}$
1030	$3.0299 \cdot 10^{-5}$	$8.6334 \cdot 10^{-1}$	$2.4847 \cdot 10^{+0}$	$2.4847 \cdot 10^{+0}$	$2.2312 \cdot 10^{-1}$	$2.7088 \cdot 10^{-1}$
1045	$2.8168 \cdot 10^{-5}$	$8.3183 \cdot 10^{-1}$	$2.3825 \cdot 10^{+0}$	$2.3825 \cdot 10^{+0}$	$2.1448 \cdot 10^{-1}$	$2.5940 \cdot 10^{-1}$
1060	$2.6209 \cdot 10^{-5}$	$8.0401 \cdot 10^{-1}$	$2.2926 \cdot 10^{+0}$	$2.2926 \cdot 10^{+0}$	$2.0693 \cdot 10^{-1}$	$2.4928 \cdot 10^{-1}$
1165	$1.6156 \cdot 10^{-5}$	$6.7477 \cdot 10^{-1}$	$1.8795 \cdot 10^{+0}$	$1.8795 \cdot 10^{+0}$	$1.7274 \cdot 10^{-1}$	$2.0217 \cdot 10^{-1}$
1210	$1.3265 \cdot 10^{-5}$	$6.4052 \cdot 10^{-1}$	$1.7707 \cdot 10^{+0}$	$1.7707 \cdot 10^{+0}$	$1.6400 \cdot 10^{-1}$	$1.8955 \cdot 10^{-1}$
1250	$1.1183 \cdot 10^{-5}$	$6.1627 \cdot 10^{-1}$	$1.6937 \cdot 10^{+0}$	$1.6937 \cdot 10^{+0}$	$1.5792 \cdot 10^{-1}$	$1.8052 \cdot 10^{-1}$
1355	$7.2763 \cdot 10^{-6}$	$5.7094 \cdot 10^{-1}$	$1.5487 \cdot 10^{+0}$	$1.5487 \cdot 10^{+0}$	$1.4689 \cdot 10^{-1}$	$1.6326 \cdot 10^{-1}$
1425	$5.5361 \cdot 10^{-6}$	$5.5039 \cdot 10^{-1}$	$1.4820 \cdot 10^{+0}$	$1.4820 \cdot 10^{+0}$	$1.4212 \cdot 10^{-1}$	$1.5512 \cdot 10^{-1}$
1500	$4.1734 \cdot 10^{-6}$	$5.3389 \cdot 10^{-1}$	$1.4275 \cdot 10^{+0}$	$1.4275 \cdot 10^{+0}$	$1.3846 \cdot 10^{-1}$	$1.4832 \cdot 10^{-1}$

Table 9: Percentage differences at NLO for $g_z = 0.2$

$ \sigma_{nnlo}^{SM} - \sigma_{nnlo}^i /\sigma_{nnlo}^{SM}\%$, $M'_Z = 800$, $g_z = 0.2$, $\tan\beta = 40$, Candia evol.						
Q [GeV]	$\sigma_{nnlo}^{SM}(Q)$ [pb/GeV]	$\Delta_{nnlo}^{FFM}\%$	$\Delta_{nnlo}^{B-L}\%$	$\Delta_{nnlo}^{q+u}\%$	$\Delta_{nnlo}^{10+5}\%$	$\Delta_{nnlo}^{d-u}\%$
1000	$3.6546 \cdot 10^{-5}$	$9.2821 \cdot 10^{-1}$	$2.7182 \cdot 10^{+0}$	$2.7182 \cdot 10^{+0}$	$2.3947 \cdot 10^{-1}$	$2.9909 \cdot 10^{-1}$
1015	$3.3935 \cdot 10^{-5}$	$8.8720 \cdot 10^{-1}$	$2.5829 \cdot 10^{+0}$	$2.5829 \cdot 10^{+0}$	$2.2804 \cdot 10^{-1}$	$2.8397 \cdot 10^{-1}$
1030	$3.1537 \cdot 10^{-5}$	$8.5154 \cdot 10^{-1}$	$2.4661 \cdot 10^{+0}$	$2.4661 \cdot 10^{+0}$	$2.1821 \cdot 10^{-1}$	$2.7085 \cdot 10^{-1}$
1045	$2.9334 \cdot 10^{-5}$	$8.2026 \cdot 10^{-1}$	$2.3642 \cdot 10^{+0}$	$2.3642 \cdot 10^{+0}$	$2.0966 \cdot 10^{-1}$	$2.5938 \cdot 10^{-1}$
1060	$2.7306 \cdot 10^{-5}$	$7.9263 \cdot 10^{-1}$	$2.2747 \cdot 10^{+0}$	$2.2747 \cdot 10^{+0}$	$2.0218 \cdot 10^{-1}$	$2.4925 \cdot 10^{-1}$
1165	$1.6888 \cdot 10^{-5}$	$6.6409 \cdot 10^{-1}$	$1.8626 \cdot 10^{+0}$	$1.8626 \cdot 10^{+0}$	$1.6826 \cdot 10^{-1}$	$2.0214 \cdot 10^{-1}$
1210	$1.3884 \cdot 10^{-5}$	$6.2993 \cdot 10^{-1}$	$1.7540 \cdot 10^{+0}$	$1.7540 \cdot 10^{+0}$	$1.5955 \cdot 10^{-1}$	$1.8952 \cdot 10^{-1}$
1250	$1.1718 \cdot 10^{-5}$	$6.0571 \cdot 10^{-1}$	$1.6769 \cdot 10^{+0}$	$1.6769 \cdot 10^{+0}$	$1.5347 \cdot 10^{-1}$	$1.8049 \cdot 10^{-1}$
1355	$7.6472 \cdot 10^{-6}$	$5.6024 \cdot 10^{-1}$	$1.5317 \cdot 10^{+0}$	$1.5317 \cdot 10^{+0}$	$1.4237 \cdot 10^{-1}$	$1.6323 \cdot 10^{-1}$
1425	$5.8293 \cdot 10^{-6}$	$5.3951 \cdot 10^{-1}$	$1.4647 \cdot 10^{+0}$	$1.4647 \cdot 10^{+0}$	$1.3751 \cdot 10^{-1}$	$1.5509 \cdot 10^{-1}$
1500	$4.4031 \cdot 10^{-6}$	$5.2277 \cdot 10^{-1}$	$1.4098 \cdot 10^{+0}$	$1.4098 \cdot 10^{+0}$	$1.3374 \cdot 10^{-1}$	$1.4828 \cdot 10^{-1}$

Table 10: Percentage differences at NNLO for $g_z = 0.2$

$d\sigma^{nnlo}/dQ$ [pb/GeV] for the FF model with $M_{Z'} = 2.5$ TeV, $\tan\beta = 40$, Candia evol.						
Q [TeV]	$g_z = 0.1$	$g_z = 0.4$	$g_z = 0.6$	$g_z = 0.8$	$g_z = 1$	$\sigma_{nnlo}^{SM}(Q)$
2.400	$2.6475 \cdot 10^{-7}$	$3.3941 \cdot 10^{-7}$	$5.0947 \cdot 10^{-7}$	$8.7995 \cdot 10^{-7}$	$1.5720 \cdot 10^{-6}$	$2.6141 \cdot 10^{-7}$
2.423	$2.4961 \cdot 10^{-7}$	$3.5212 \cdot 10^{-7}$	$6.0291 \cdot 10^{-7}$	$1.1654 \cdot 10^{-6}$	$2.2223 \cdot 10^{-6}$	$2.4543 \cdot 10^{-7}$
2.446	$2.3629 \cdot 10^{-7}$	$4.0068 \cdot 10^{-7}$	$8.4077 \cdot 10^{-7}$	$1.8529 \cdot 10^{-6}$	$3.7317 \cdot 10^{-6}$	$2.3050 \cdot 10^{-7}$
2.469	$2.2656 \cdot 10^{-7}$	$6.0047 \cdot 10^{-7}$	$1.7162 \cdot 10^{-6}$	$4.2536 \cdot 10^{-6}$	$8.5322 \cdot 10^{-6}$	$2.1654 \cdot 10^{-7}$
2.492	$2.4932 \cdot 10^{-7}$	$3.7446 \cdot 10^{-6}$	$1.2697 \cdot 10^{-5}$	$2.3281 \cdot 10^{-5}$	$3.0409 \cdot 10^{-5}$	$2.0349 \cdot 10^{-7}$
2.5000	$3.7947 \cdot 10^{-5}$	$3.7947 \cdot 10^{-5}$	$3.7947 \cdot 10^{-5}$	$3.7947 \cdot 10^{-5}$	$3.7947 \cdot 10^{-5}$	$1.9900 \cdot 10^{-7}$
2.5003	$8.5271 \cdot 10^{-6}$	$3.7283 \cdot 10^{-5}$	$3.7757 \cdot 10^{-5}$	$3.7858 \cdot 10^{-5}$	$3.7892 \cdot 10^{-5}$	$1.9886 \cdot 10^{-7}$
2.5005	$2.7949 \cdot 10^{-6}$	$3.5983 \cdot 10^{-5}$	$3.7438 \cdot 10^{-5}$	$3.7730 \cdot 10^{-5}$	$3.7824 \cdot 10^{-5}$	$1.9873 \cdot 10^{-7}$
2.5770	$1.5907 \cdot 10^{-7}$	$1.4769 \cdot 10^{-7}$	$2.2368 \cdot 10^{-7}$	$5.0120 \cdot 10^{-7}$	$1.1340 \cdot 10^{-6}$	$1.6192 \cdot 10^{-7}$
2.636	$1.3692 \cdot 10^{-7}$	$1.2412 \cdot 10^{-7}$	$1.3364 \cdot 10^{-7}$	$1.9772 \cdot 10^{-7}$	$3.6561 \cdot 10^{-7}$	$1.3839 \cdot 10^{-7}$
2.700	$1.1628 \cdot 10^{-7}$	$1.0680 \cdot 10^{-7}$	$1.0536 \cdot 10^{-7}$	$1.2481 \cdot 10^{-7}$	$1.8637 \cdot 10^{-7}$	$1.1718 \cdot 10^{-7}$

Table 11: NNLO cross sections for the FF model with a $M_{Z'} = 2.5$ TeV for values of the coupling constant g_z larger than $g_z = 0.1$

References

- [1] For reviews and references therein see *e.g.*:
P. Langacker, arXiv:0801.1345 ;
T.G. Rizzo, hep-ph/0610104 ;
A. Leike, *Phys. Rep.* **317** (1999) 143;
Yu.Ya.Komachenko and M.Yu.Khlopov, *Sov. J. Nucl. Phys.* **51** (1990) 692, *Yad. Fiz.* **51** (1990) 1081.
- [2] A.E. Faraggi and D.V. Nanopoulos, *Mod. Phys. Lett.* **A6** (1991) 61;
A.E. Faraggi, *Phys. Lett.* **B499** (2001) 147.
- [3] J. Pati, *Phys. Lett.* **B388** (1996) 532.
- [4] C. Corianò, A.E. Faraggi and M. Guzzi, *The Eur. Phys. Jour.* **C53** (2008) 701;
Hye-Sung Lee, arXiv:0802.0506 [hep-ph].
- [5] A.E. Faraggi, *Int. J. Mod. Phys.* **A19** (2004) 5523; hep-th/9910042; hep-ph/9707311.
- [6] I. Antoniadis, J. Ellis, J. Hagelin and D.V. Nanopoulos *Phys. Lett.* **B231** (1989) 65.
- [7] I. Antoniadis, G.K. Leontaris and J. Rizos, *Phys. Lett.* **B245** (1990) 161.
- [8] A.E. Faraggi, *Phys. Lett.* **B278** (1992) 131; *Phys. Lett.* **B274** (1992) 47; *Nucl. Phys.* **B387** (1992) 239; *Nucl. Phys.* **B403** (1993) 101; *Phys. Rev.* **D47** (1993) 5021; *Phys. Lett.* **B377** (1996) 43; *Nucl. Phys.* **B487** (1997) 55;
G.B. Cleaver, A.E. Faraggi and D.V. Nanopoulos, *Phys. Lett.* **B455** (1999) 135; *Int. J. Mod. Phys.* **A16** (2001) 425;
G.B. Cleaver, A.E. Faraggi, D.V. Nanopoulos and J.W. Walker, *Nucl. Phys.* **B593** (2001) 471; *Nucl. Phys.* **B620** (2002) 259;
A.E. Faraggi, E. Manno and C. Timirgaziu, *The Eur. Phys. Jour.* **C50** (2007) 701.
- [9] G.B. Cleaver, A.E. Faraggi and C. Savage, *Phys. Rev.* **D63** (2001) 066001;
G.B. Cleaver, D.J. Clements and A.E. Faraggi, *Phys. Rev.* **D65** (2002) 106003.
- [10] M. Carena, A. Daleo, B.A. Dobrescu and T.M. Tait, *Phys. Rev.* **D70** (2004) 093009.
- [11] R. Hamberg, W.L. van Neerven, T. Matsuura, *Nucl. Phys.* **B359** (1991) 343,
Erratum-ibid.**B 644** (2002) 403.
- [12] T. Appelquist, B.A. Dobrescu and A.R. Hopper, *Phys. Rev.* **D68** (2003) 035012.

- [13] Hye-Sung Lee, Konstantin T. Matchev, Ting T. Wang, *Phys. Rev.* **D77** (2008) 015016; Paul G. Langacker, Gil Paz, Lian-Tao, Wang, arXiv:0710.1632 [hep-ph]; Paul G. Langacker, Gil Paz, Lian-Tao, Wang, arXiv:0801.3693 [hep-ph];
- [14] C. Corianò, N. Irges and S. Morelli, *JHEP* **0707**, (2007) 008.
- [15] C. Corianò, N. Irges and S. Morelli, *Nucl. Phys.* **B789** (2008) 133.
- [16] R. Armillis, C. Corianò and M. Guzzi "Trilinear Anomalous Gauge Interactions from Intersecting Branes and the Neutral Currents Sector", arXiv:0711.3424 [hep-ph].
- [17] C. Corianò, M. Guzzi and S. Morelli, "Unitarity Bounds for Gauged Axionic Interactions and the Green-Schwarz Mechanism", arXiv:0801.2949 [hep-ph].
- [18] F. Petriello and S. Quackenbush, arXiv:0801.4389 [hep-ph].
- [19] A. Cafarella, C. Corianò and M. Guzzi, *Nucl. Phys.* **B748** (2006) 253.
- [20] A. Cafarella, C. Corianò and M. Guzzi, *JHEP* **0708**, (2007) 030.
- [21] A.D. Martin, R.G. Roberts, W.J. Stirling, R.S. Thorne *The Eur. Phys. Jour.* **C23** (2002) 73, *Phys. Lett.* **B531** (2002) 216
- [22] <http://www.le.infn.it/candia/>